Palaeogeography, Palaeoclimatology, Palaeoecology 310 (2011) 191–205

Contents lists available at ScienceDirect

Palaeogeography, Palaeoclimatology, Palaeoecology

journal homepage: www.elsevier.com/locate/palaeo

Okhotsk Sea ice coverage and Kamchatka glaciation over the last 350 ka — Evidence from ice-rafted debris and planktonic $\delta^{18}O$

Dirk Nürnberg [a,*], Dirk Dethleff [b,1], Ralf Tiedemann [c,2], André Kaiser [a], Sergey A. Gorbarenko [d,3]

[a] Leibniz-Institut für Meereswissenschaften (IfM-GEOMAR), Wischhofstrasse 1-3, D-24148 Kiel, Germany
[b] Institute for Polar Ecology, University of Kiel, Wischhofstrasse 1-3, Geb. 12, D-24148 Kiel, Germany
[c] Alfred-Wegener-Institute for Polar and Marine Research, Columbusstrasse, D-27568 Bremerhaven, Germany
[d] V.I. Il'ichev Pacific Oceanological Institute FEB RAS, 43 Baltiskaya Street, 690041 Vladivostok, Russia

ARTICLE INFO

Article history:
Received 13 December 2010
Received in revised form 6 July 2011
Accepted 10 July 2011
Available online 20 July 2011

Keywords:
Okhotsk Sea
Ice rafted debris
Kamchatka glaciation
Foraminiferal oxygen isotopes
Marine Isotope Stage 6

ABSTRACT

High-resolution records of ice-rafted debris (IRD) and oxygen isotope records spanning an E–W-trending transect across the Okhotsk Sea unravel the marine and terrestrial cryogenic history of NE-Siberia over the last 350 kyr. IRD, predominantly dispersed basin-wide by sea-ice, shows lowest fluxes during interglacial periods implying a reduced and seasonal sea-ice coverage. Highest IRD accumulation rates are observed during glacial and deglacial periods with a more extended, but highly dynamic ice cover. Although being rather synchronous, IRD fluxes are on average higher in the western Okhotsk Sea than in the eastern part, pointing to a persistent but mobile, particle-supplying sea-ice cover even during full glacial conditions, presumably less dense in the eastern parts. MIS 6 is exceptional in this respect: Asynchronous fluxes of IRD, which vary spatially, reflect rapid paleoclimatic and paleo-glaciomarine changes. IRD accumulation rates were by factor 2–3 higher during MIS 6 as compared to the last glacial maximum, and the IRD depositional center shifted from the western Okhotsk Sea (early MIS 6) toward Kamchatka (late MIS 6), synchronous to a distinct change in the IRD mineral composition. Both, the characteristic composition of late MIS 6 IRD originating from the Sredinny Mountain Range of Kamchatka and their significantly enhanced accumulation rates refer to intensified iceberg dispersal across the eastern part of the Okhotsk Sea at ~138 ka, ~135 ka, ~129 ka, and ~128 ka BP. This scenario affords the presence of extended mountain glaciers protruding down to sea level on the western side of Kamchatka. Anomalously light planktonic stable oxygen isotopes during MIS 6.3, Termination II and MIS 5.5–5.4 suggest significant freshwater supply related to the westward drainage of Kamchatka glaciers. The intensified Kamchatka glaciation observed during late MIS 6 was repeated during MIS 3. Iceberg discharges into the eastern Okhotsk Sea are observed at ~60 ka, ~51 ka, ~42 ka, ~38 ka, ~36 ka, and ~31 ka, and may partly correspond to N-Atlantic Heinrich Events.

1. Introduction

The late Quaternary climatic conditions and glaciomarine changes in the Okhotsk Sea (Fig. 1) are still a matter of debate. Deduced from terrestrial and shallow marine morphological studies, Grosswald (1998) and Grosswald and Hughes (1998) suggested large ice-sheets covering the entire Okhotsk Sea during the late Pleistocene glacial cycles, a theory which was finally refuted. Other studies proposed rather spatially limited ice sheets (Bigg et al., 2008), temporal mountain glaciations on the surrounding hinterland, and predominating sea-ice coverage during the Last Glacial Maximum (LGM) and mid Pleistocene (e.g Frenzel et al., 1992; Zech et al., 1996, 1997; Bäumler and Zech, 2000; Shiga and Koizumi, 2000; Brigham-Grette et al., 2003; Okazaki et al., 2003; Nürnberg and Tiedemann, 2004; Okazaki et al., 2005; Sakamoto et al., 2005).

Drifting sea-ice represents a proven geological agent to dislocate ice-rafted debris (IRD) consisting of terrigenous components of varying grain sizes from shore sources to deep-sea sinks in north polar seas (e.g. Kempema et al., 1989; Reimnitz et al., 1993a; Nürnberg et al., 1994; Dethleff et al., 2000; Eicken et al., 2000; Hebbeln, 2000; Darby, 2003; Dethleff, 2005; Dethleff and Kuhlmann, 2010). Paleo sea-ice expansion in the Okhotsk Sea is commonly reconstructed from coarse lithic terrestrial particles >63 µm, hereafter referred to as sea-ice supplied IRD ($IRD_{sea\text{-}ice}$) (e.g. Gorbarenko et al., 2002; Sakamoto et al., 2003, 2005). Based on a 1.1 million year record from the central Okhotsk Sea, Nürnberg and Tiedemann (2004) proposed that terrigenous material of continental origin dominates the glacial sedimentation in the Okhotsk Sea, with sea ice rafting from

* Corresponding author. Tel.: +49 431 600 2313; fax: +49 431 600 2925.
E-mail addresses: dnuernberg@ifm-geomar.de (D. Nürnberg), ddethleff@ipoe.uni-kiel.de (D. Dethleff), Ralf.Tiedemann@awi.de (R. Tiedemann), gorbarenko@poi.dvo.ru (S.A. Gorbarenko).
[1] Tel.: +49 431 600 1267; fax: +49 431 600 1210.
[2] Tel.: +49 471 4831 1200; fax: +49 471 4831 1923.
[3] Tel.: +7 4232 3123 82; fax: +7 4232 3125 73.

0031-0182/$ – see front matter
doi:10.1016/j.palaeo.2011.07.011

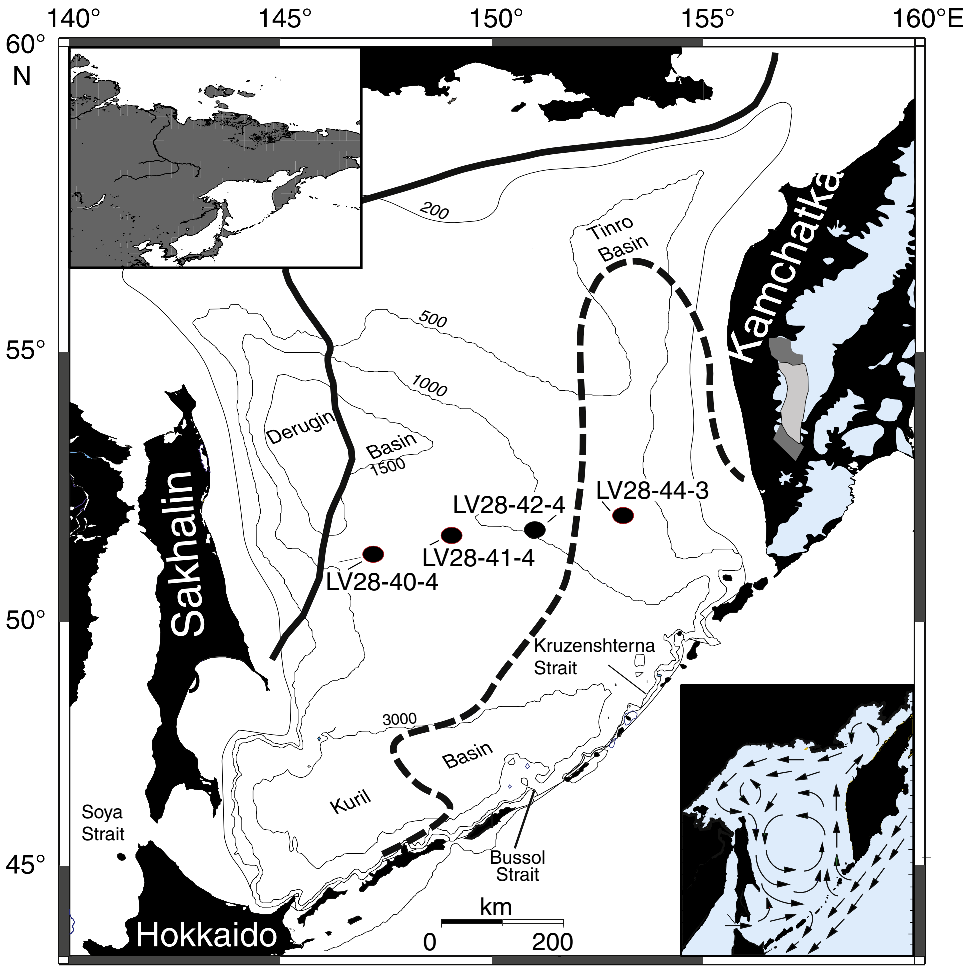

Fig. 1. Bathymetric chart of the Okhotsk Sea (NW Pacific), showing locations of sediment cores studied here (bathymetry in meters). Modern January sea-ice extent (solid bold line) and the maximum sea-ice coverage during March (dashed bold line) according to NASA Nimbus 7 and Parkinson et al. (1987) are indicated. On Kamchatka peninsula, the metasedimentary and metavolcanic rocks (dark-gray areas) and felsic paragneisses (light-gray area) of the Sredinny Mountain Range (after Bindemann et al., 2002) represent potential terrestrial source areas for $IRD_{iceberg}$. Light blue area indicates the maximal Quaternary glaciation according to Zamoruyev (2004). Inlet in lower right corner shows modern cyclonic oceanic surface circulation pattern, inlet in upper left corner provides larger view of eastern Asia.

coastal sources appearing to be the most likely and effective transport agent. This notion is supported by later studies, which deduced partly heavy and perennial ice conditions during full glacial times from the terrigenous and biogenous particle content in deep Okhotsk Sea sediments (e.g., Liu et al., 2006; Wang and Wang, 2008). In contrast to the Okhotsk Sea, studies on North Pacific sediment records identified formerly glaciated terrestrial regions as source areas of IRD, and defined the advance of icebergs as the major IRD supplying agent to the remote NW-Pacific (e.g., von Huene et al., 1973; Rea, 1994; Hewitt et al., 1997; St. John and Krissek, 1999). Iceberg-related IRD is hereafter referred to as $IRD_{iceberg}$.

The intention of our study is to decipher the marine and terrestrial cryogenic development of the central Okhotsk Sea area including parts of the Kamchatka Peninsula over the past 350 ka (MIS 1–10). Supported by planktonic oxygen isotope records, we systematically study IRD-distribution patterns across the Okhotsk Sea to assess the role of sea-ice and iceberg transport for the supply of terrigenous material to the Okhotsk Sea.

2. Okhotsk Sea environmental settings

Bordered by the Asian continent and Sakhalin Island to the northwest and north, and the Kurile-Kamchatka-Island Arc to the east and southeast, the Okhotsk Sea is the second largest marginal sea of the Pacific (Fig. 1). The straits between the Kurile Islands connect the Okhotsk Sea to the Pacific Ocean. Tatarsky and Soya straits link the Okhotsk Sea to the Japan Sea in the west and southwest. The broad, shallow northern and northeastern Okhotsk Sea shelves slope toward the extended Deryugin and Kurile Basins in the south, and toward the shallower and smaller Tinro Basin west off Kamchatka.

The present-day surface circulation is characterized by a large cyclonic gyre fed by the inflow of relatively warm and saline Pacific water masses through Kruzenshterna Strait (Fig. 1). This Pacific intrusion contributes to the northward directed West Kamchatka Current, which additionally mixes with partly re-circulating water masses from the East Sakhalin Current and with water from the broad northern shelf areas (e.g., Leonov, 1960; Moroshkin, 1966; Alfutis and Martin, 1987). Further gyre-feeding saline surface waters intrude from the Sea of Japan through Soya Strait. The Okhotsk surface waters are characterized by salinities between 32 and 34, while lower salt contents of 20 to 25 are restricted to areas influenced by the Amur River discharge around the northern tip of Sakhalin Island (Watanabe and Wakatsuchi, 1998; Gladyshev et al., 2003). During winter, intense sea-ice formation on the western, northern and eastern Okhotsk Sea shelves cause the generation of dense water (Martin et al., 1998; Gladyshev et al., 2003; Shcherbina et al., 2003), which is suggested to contribute to the formation and ventilation of the North Pacific Intermediate Water (NPIW) (e.g. Ohtani and Nagata, 1990; Riser, 1990; Talley, 1991; Wong et al., 1998).

The Okhotsk Sea meteorology and climate are strongly influenced by the surrounding NE-Siberian landmasses. Extremely cold winter air temperatures as low as −32 °C (Wakatsuchi and Martin, 1990) indicate a pronounced polar climatic regime, which is driven by the interaction of the strong continental Siberian High and the marine Aleutian Low (Parkinson, 1990; Tchaibana et al., 1996; Ponomorev et al., 1999). Strong and cold northerly winds affect the sea-surface temperature and promote sea-ice formation during winter. The cold winter season is contrasted by warm summers resulting in recurring water temperatures of as high as 6–12 °C (Zenkevitch, 1963) caused by the interrelationship between the South-Asian Low and the North Pacific (Hawaiian) High (Wang and Li, 1990).

From November through May, the Okhotsk Sea is widely covered by sea-ice with a maximum thickness of ~1 m (Gloersen et al., 1992; Fig. 1). In the western part of the Okhotsk Sea, the first-year drift ice cover extends far south to 45°N. The extreme ice extent is related to the geographically protected nature of the sea, which promotes earlier seasonal formation and later breakup of sea-ice as compared to other marine areas of the same latitude (Parkinson et al., 1987). Okhotsk freeze-up starts in the northwestern part of the sea, where low fall atmospheric temperatures, shallow water depths, and related lower sensible heat content of the water column are the driving mechanisms for initial sea-ice formation. Extended recurrent and new-ice producing shore polynyas appear in direct vicinity to the coastal interface along the Okhotsk Siberian mainland, and off Kamchatka and Sakhalin, (e.g. Parkinson and Gratz, 1983; Alfutis and Martin, 1987; Gladyshev et al., 2000; Polyakov and Martin, 2000). Okhotsk sea-ice does not survive the melt season, and the basin is ice-free from June/July through the end of October, when freeze-up starts again.

3. Material and methods

3.1. Sediment cores and chronostratigraphy

We focus on a W–E trending core-transect across the Okhotsk Sea at ~52°N (Fig. 1, Table 1). The piston cores from ~680 to 1370 m water depth were recovered during RV Lavrentiev cruise LV28 in 1998 (Biebow and Hütten, 1999). The chronostratigraphic framework of the cores covering the last ~350 kyr is based on stable isotopes ($\delta^{18}O$) and accelerator mass spectrometry radiocarbon datings (AMS^{14}C). Stable $\delta^{18}O$ isotope analyses were performed on 10–20 specimens of the planktonic foraminifer *Neogloboquadrina pachyderma* sinistral selected from the 125–250 μm size fraction. Additional $\delta^{18}O$ measurements were carried out on 2–3 specimens of the endobenthic foraminifer *Uvigerina auberiana* in cores LV28-44-3 and LV28-42-4. Since we did not obtain any interspecies $\delta^{18}O$-offset in parallel analyses between *U. auberiana* and other foraminifers like *U. peregrina*, *U. senticosa* and *U. angulosa*, the latter three species were used for the development of our benthic $\delta^{18}O$ age scales in cases of rare abundances of *U. auberiana* in the deposits. The isotopic analyses were performed at IFM-GEOMAR (Kiel) on a Finnigan MAT 252 mass spectrometer coupled with the automated Kiel carbonate preparation line (Kiel CARBO II device) after ultrasonic cleaning of the foraminiferal tests in distilled water. The mass spectrometer is calibrated to NBS 19 (National Bureau of Standards), and the isotope values are reported on the VPDB (Vienna PDB) scale. The standard deviation is <0.06‰ for $\delta^{18}O$.

Four AMS^{14}C ages in the uppermost section of core LV28-42-4 provided additional stratigraphic information (Nürnberg and Tiedemann, 2004). The measurements were carried out on planktonic foraminiferal tests (1000–2000 species of *N. pachyderma* sin.) obtained from the 125–250 μm fraction. The AMS^{14}C analyses were performed at the Leibniz Laboratory for Radiometric Dating and Isotope Research at Kiel. After applying a marine reservoir effect of 1000 years for planktonic ^{14}C ages according to Southon et al. (1993), Gorbarenko et al. (2000), and Yoneda et al. (2000), all radiocarbon dates were converted to calendar years using the CALIB 4.1.2 calibration program of Stuiver and Reimer (1993).

Our $\delta^{18}O$ stratigraphy is based on the graphic correlation of the planktonic and benthic oxygen isotope curves to the Bassinot et al. (1994) $\delta^{18}O$ reference stack (Fig. 2). The correlation was performed with the program AnalySeries Version 1.1 (Paillard et al., 1996). As the isotope data of core LV28-41-4 show unusually low planktonic $\delta^{18}O$ values in early MIS 6, additional age control was derived from the correlation of magnetic susceptibility records of cores LV28-41-4 and LV28-42-4 (Fig. 2). Marine oxygen isotope events (MIS) were recognized using the nomenclature proposed by Tiedemann et al. (1994) and Prell et al. (1986). According to the established stratigraphy, the central Okhotsk Sea cores LV28-41-4 and LV28-42-4 cover MIS 1–10, while the shorter cores LV20-40-4 and LV28-44-3 reach down to upper and middle MIS 6.

Table 1
Core information (RV A. Lavrentyev cruise in 1998).

Core No.	Recovery (cm)	Water depth (m)	Longitude	Latitude
LV28-40-4	979	1370	147°11.647′E	51°20.141′N
LV28-41-4	981	1082	149°04.084′E	51°40.512′N
LV28-42-4	1084	1041	150°59.125′E	51°42.886′N
LV28-44-3	1112	684	153°05.949′E	52°02.514′N

3.2. Assessing the portion of IRD

As no hints for turbidity currents or gravity flows were identified in the sediment cores (Nürnberg et al., 1997; Biebow and Hütten, 1999), and additionally, particle sizes of volcanic ash layers found in Okhotsk Sea and northern Pacific sediment cores range between silt and fine-sand (Ninkovitch et al., 1966; Kaiser, 2000), we imply that coarse lithic grains identified in Okhotsk Sea deposits must have been supplied by ice transport. Following the approach of Nürnberg and Tiedemann (2004), we here define the lithic (carbonate-free) 125–500 μm size fraction as IRD_{total}.

The >63 μm fraction was separated from the bulk sediment sample by wet sieving, and subsequently subdivided through sonic sifting after drying at 40 °C into five sub-fractions (63–125 μm; 125–250 μm; 250–500 μm; 500–1000 μm; >1000 μm, hereinafter 'pebble'). The fractions were weighted, and weight percentages were calculated. We neglected the >1000 μm 'pebble'-sized material in our calculations in order to avoid misleading peak values caused by the sporadic occurrence of individual pebbles. Finally, we converted the weight of the four remaining sub-fractions to percentages of the 'pebble-free' coarse fraction.

Various IRD components were identified from the size class 125–500 μm, providing important provenance information. Between 400 and 500 grains were randomly selected from each sample from representative splits, counted, and presented as grain percentages (gr.% = grains of $IRD_{component}$ per IRD_{total}). Rock fragments (composed of various minerals), quartz, dark minerals (mainly pyroxene and hornblende), and feldspar were differentiated and considered as total IRD_{total}. As feldspar in core LV2840-4, and feldspar and dark minerals in core LV28-41-4 are absent, IRD_{total} in these cases is represented by the percentages of the remaining IRD components. Dark minerals are typically brownish-green to dark green to black. The roundness of the quartz grains describing the sharpness of the grain's edges and corners regardless of shape, is differentiated into angular to well rounded grains according to the scheme of Pettijohn et al. (1972).

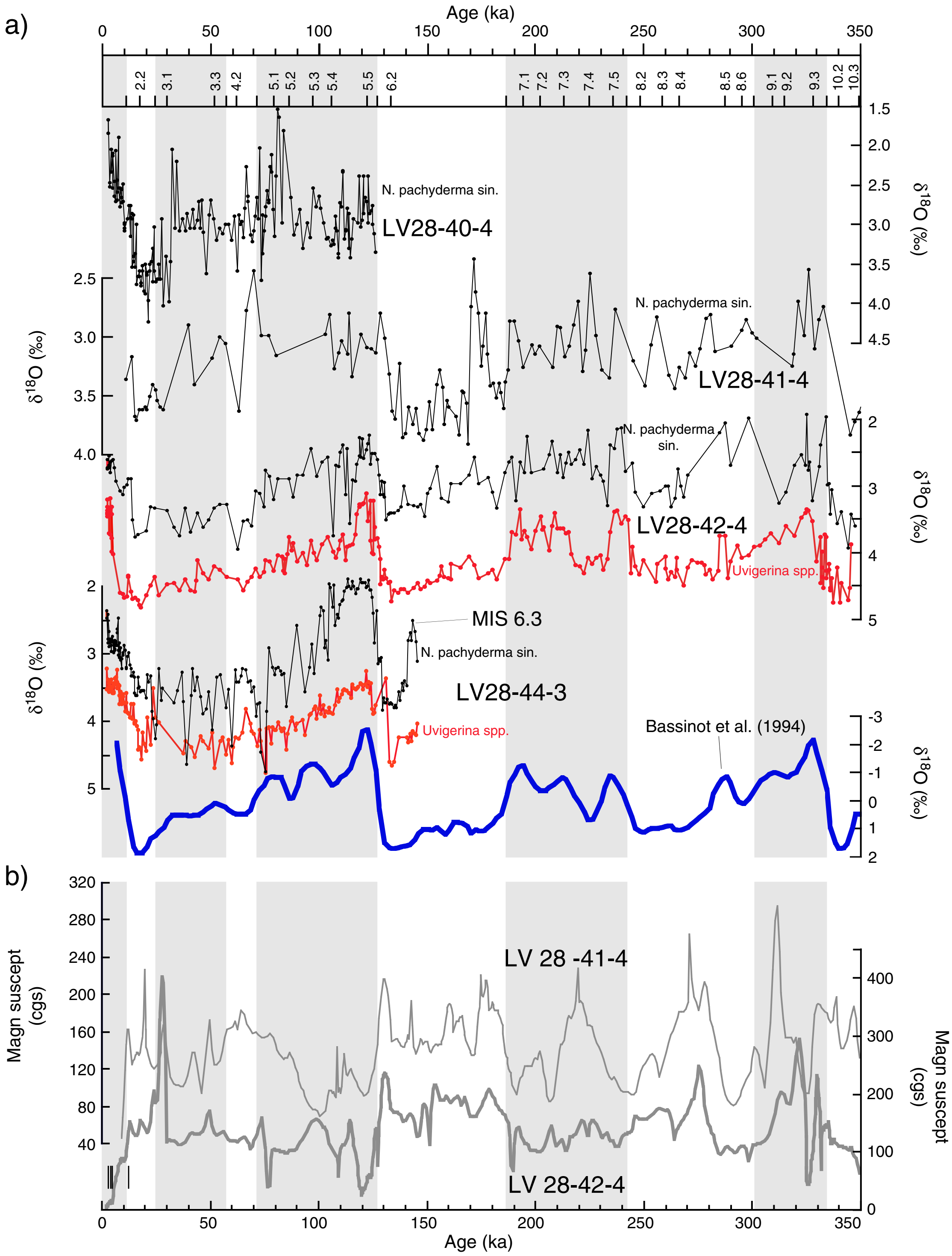

Fig. 2. Stratigraphic framework of the Okhotsk Sea core transect (a). Black curves represent planktonic $\delta^{18}O$ records (*N. pachyderma* sin.), while red curves are benthic $\delta^{18}O$ data (*Uvigerina* spp.). The benthic $\delta^{18}O$ records were tuned to that of core LV28-42-4. For core LV28-42-4, Nürnberg and Tiedemann (2004) established the chronostratigraphy based on benthic isotopes tuned to the Bassinot et al. (1994) isotope reference record (thick blue line), and on AMS ^{14}C-dating in the uppermost core section (black lines at top of the magnetic susceptibility record). Additional age control for core LV28-41-4 was derived by correlating the magnetic susceptibility record to that of core LV28-42-4 (b). Shaded areas mark interglacial periods.

3.3. Quantification of flux rates

The paleo-flux of IRD_{total} and individual grain components is expressed by accumulation rates (AR in g cm^{-2} kyr^{-1}). The bulk accumulation rate (AR_{bulk}) was described by van Andel et al. (1975) as

$$AR_{bulk} = LSR \times D_{bulk} \quad (1)$$

where the dry bulk density (D_{bulk} in g cm^{-3}) was derived by weighing a defined sample volume before and after freeze-drying. The linear sedimentation rate (LSR, in cm kyr^{-1}) (Fig. 3) was calculated by dividing the sediment thickness between two age control points by the time required for its deposition. Sedimentation rates are generally low in the central Okhotsk Sea (LV28-41-4, LV28-42-4), and vary from ~2–5 cm kyr^{-1} for most of the time covered. The two shorter cores

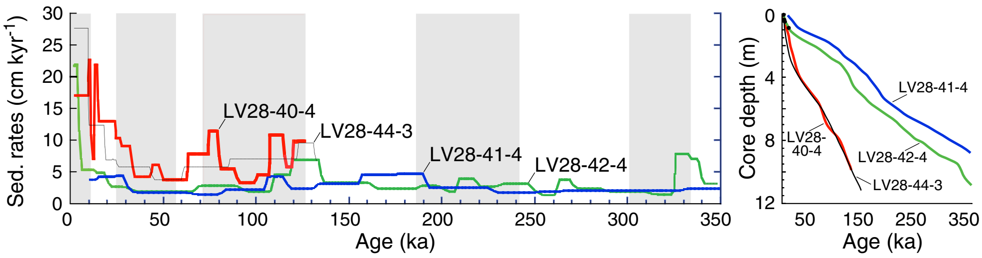

Fig. 3. Comparison of sedimentation rates *versus* age (left), and depth *versus* age diagram (right). LV28-40-4 (red), LV28-41-4 (blue), LV28-42-4 (green), and LV28-44-3 (black). Shaded areas mark interglacial periods. AMS^{14}C-datings in the uppermost section of core LV28-42-4 (Nürnberg and Tiedemann, 2004) are marked by black dots.

(LV28-40-4, LV28-44-3) close to Sakhalin and Kamchatka, respectively, show higher sedimentation rates mostly varying between 4 and 13 cm kyr^{-1}. During pronounced interglacial periods and glacial–interglacial transitions, the sedimentation rates increase at all sites, reaching maximum values of >25 cm kyr^{-1} in core LV28-44-3.

We assessed the flux rate of the pebble-free sand fraction (>63 µm, <1000 µm) using

$$AR_{sand} = (AR_{bulk} \times wt.\%_{sand}) \times 100^{-1} \quad (2)$$

where wt.%$_{sand}$ comprises the summarized weight percentages of the >63 µm size fractions (without pebbles) related to the weight of the bulk sample. We calculated the flux rate of the 125–500 µm fraction (defined as the size fraction transported by ice) as

$$AR_{125-500\mu m} = AR_{sand} \times \left(wt.\%_{125-500\mu m} \times 100^{-1}\right). \quad (3)$$

Finally, we estimated the flux rates of IRD$_{total}$ and of individual IRD components (IRD$_{component}$) following Krissek and St. John's (2002) approach by multiplying the AR$_{125–500µm}$ with the grain percentages of IRD$_{total}$, and the grain percentages of the individual IRD components using the equations

$$AR\ IRD_{total} = \left(AR_{125-500\mu m} \times gr.\%IRD_{total}\right) \times 100^{-1} \quad (4)$$

$$AR\ IRD_{component} = \left(AR_{125-500\mu m} \times gr.\%IRD_{component}\right) \times 100^{-1}. \quad (5)$$

4. Results

Sedimentation in the Okhotsk Sea is dominated by terrigenous, siliciclastic material. The terrigenous sequences, characterized by >85% siliciclastics and magnetic susceptibilities of 100–250 SI*10^{-5} (Figs. 2, 4) provide as much as 90% of the 125–500 µm fraction. During short deglacial to interglacial/interstadial events of enhanced marine productivity (see Nürnberg and Tiedemann, 2004), the siliciclastic sediment portion declines to less than 35%. The coarse fraction (>63 µm) in the Okhotsk Sea sediment cores varies between 1 and ~40 wt.%. The two central sites show values between 4 and 39 wt.% (average: ~15–20 wt.%), while the marginal cores reveal reduced amplitudes in coarse fraction (1–29 wt.%) and lower mean values of ~8–11 wt.%. High portions of coarse fraction are commonly related to full glacial conditions, while interglacials exhibit lower occurrences. Angular to well rounded dropstones of >2–7 cm in size commonly occur in both glacial and interglacial deposits, and point to ice-related transport processes (Fig. 5).

4.1. Total IRD

Highest IRD$_{total}$ percentages are present in the western Okhotsk Sea cores LV28-40-4 and LV28-41-4 with values between 60 and 80 gr.%, culminating at ~90 gr.% (Fig. 4). The central and eastern Okhotsk Sea sediment records have lower IRD$_{total}$ values of 50–70 gr.% in core LV28-42-4, and 40–60 gr.% in the easternmost core LV28-44-3. In all cores, enhanced IRD abundances are mainly related to glacials and their terminations, while lower IRD supply occurs during interglacial periods. Prominent minima in IRD$_{total}$ are evident during interglacial times (MIS 9, MIS 7.3–7.2, MIS 5.5–5.4, MIS 3.1, and Holocene Climatic Optimum).

Similarly, the accumulation rates of IRD$_{total}$ are enhanced during glacial periods and terminations (maximum: 0.5–0.8 g cm^{-2} kyr^{-1}), while lower particle fluxes are present during interglacials (0.02–0.34 g cm^{-2} kyr^{-1}) (Fig. 5) with lowest accumulation rates evident around MIS 5.5 and during the Holocene (<0.02 g cm^{-2} kyr^{-1}). Average IRD$_{total}$ accumulation rates decrease from the western sites (0.09–0.15 g cm^{-2} kyr^{-1}) to a value of ~0.07 g cm^{-2} kyr^{-1} at the central core, and then increase toward a mean flux rate of ~0.09 g cm^{-2} kyr^{-1} at the easternmost site off Kamchatka. Higher IRD$_{total}$ flux rates in the western Okhotsk Sea reveal that the area was repeatedly influenced by ice coverage, which is concordant to the modern high IRD flux provided by seasonal sea-ice as deduced from sediment trap studies (Sakamoto et al., 2003). The increasing mean IRD$_{total}$ accumulation rate off Kamchatka shows that the deposition history of the eastern Okhotsk Sea temporarily was also strongly influenced by ice rafted material. In all cores except site LV28-40-4, the peak IRD accumulation rates (~0.5–0.8 g cm^{-2} kyr^{-1}) during MIS 6 were by factor 2–3 higher if compared to the last glacial, and even exceeded the particle flux in MIS 3–5 and MIS 7–10 by a factor of 3 to 10 (Fig. 5). Notably, a shift of high IRD accumulation rates from early MIS 6 in the West to late MIS6/Termination II in the East is evident.

4.2. Individual IRD components

Specific IRD$_{total}$ components are present in varying abundances throughout the sedimentary records, and dominate the 125–500 µm fraction with ~50–90 gr.% (Fig. 4). Rock fragments are most abundant (35–50 gr.%) and dominate the background IRD flux in all sediment records (Figs. 4, 5). Feldspar (0–2 gr.%) is negligible in this respect. Strongly varying grain percentages and accumulation rates of dark minerals and quartz components, which are related to short-term glacial/interglacial transitions and few full glacial periods (Figs. 6, 7), allow to differentiate between depositional environments from west to east.

In the western Okhotsk Sea (LV28-40-4), quartz varies between ~1 gr.% (interglacial) and 20 gr.% (glacial), and is dominated by angular grains (Fig. 6). Dark minerals are rare (1–2 gr.%), and rounded quartz occurs only in traces (<1 gr.%). The accumulation rate of angular quartz peaks during MIS 2 (Fig. 7). At site LV28-41-4, angular quartz ranges between 4 gr.% and 34 gr.%, and correlates to IRD$_{total}$. Accumulation rates of angular quartz are relatively high (0.02 to 0.1 g cm^{-2} kyr^{-1}) with a maximum of 0.23 g cm^{-2} kyr^{-1} during early MIS 6. Rounded quartz is rare (1–3%).

In the central Okhotsk Sea (LV28-42-4), angular quartz is present throughout the deposits between 1 gr.% and 18 gr.%, the pattern of

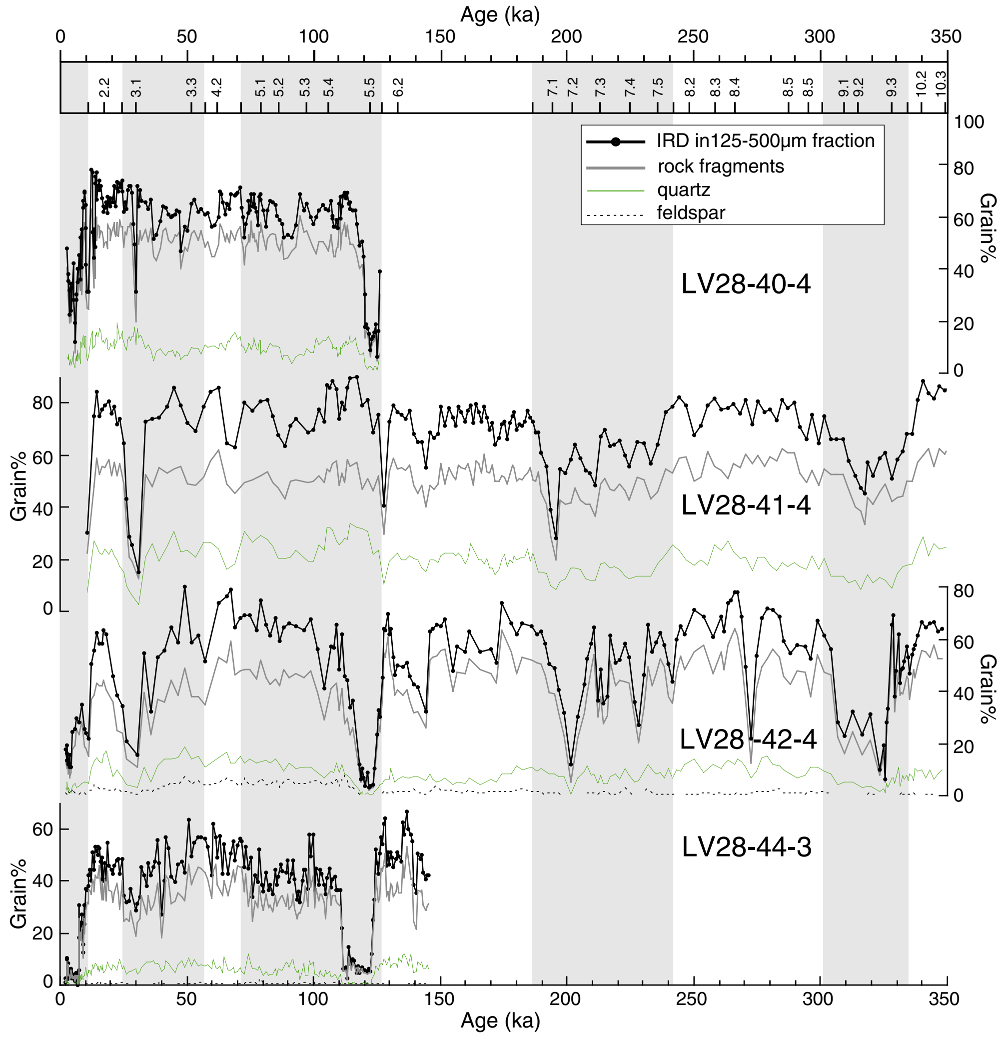

Fig. 4. Grain percentages of IRD_{total} (bold black line), and grain percentages of individual IRD components in the 125–500 µm fraction: rock fragments (bold gray line), quartz (thin green line), feldspar (dashed line). Shaded areas mark interglacial periods.

which is similar to the western Okhotsk Sea. During MIS 6, values are typically low (Fig. 6). Dark minerals range between 1 gr.% and 6 gr.% (average: ~2 gr.%), revealing clearly higher values than in the western Okhotsk Sea. In particular during periods of reduced angular quartz occurrence (MIS 6), dark minerals remain present in high abundances implying constant or even increased IRD supply from terrestrial sources. Rounded quartz is below 1–2 gr.%. Accumulation rates of angular quartz (Fig. 7) show values of >0.06 g cm^{-2} kyr^{-1} (MIS 2), and dark mineral fluxes are present with maximum ~0.02 g cm^{-2} kyr^{-1} (MIS 6). During MIS 6 and Termination II, accumulation rates of angular quartz and dark minerals clearly co-vary with the accumulation rate of IRD_{total} (Fig. 5), while the flux rate of rounded quartz is temporarily opposite (Fig. 7).

In the eastern Okhotsk Sea (LV28-44-3), the composition of IRD is significantly different from the western areas. Angular quartz is present between 1 gr.% and 11 gr.%, with an average of ~5 gr.% (Fig. 6). Dark minerals exhibit highest values (~3–4 gr.%) of all cores, temporarily exceeding angular quartz with maximum 10–14 gr.%, in particular during MIS 6 and MIS 4. During MIS 2, the abundance of dark minerals significantly decreases, while values of angular quartz remain enhanced. Rounded quartz is present on average with 1–2 gr.%, and percentages mostly vary between 1 and 3 gr.%. During MIS 6, peak values of as much as 4 gr.% represent the highest percentages of rounded quartz in the entire core transect. Accumulation rates of angular quartz (Fig. 7) amount to ~0.01 to 0.065 g cm^{-2} kyr^{-1}, and of dark minerals raise to >0.05 g cm^{-2} kyr^{-1} (MIS 6). Both fluxes culminate during late MIS 6, Termination II, and MIS 3 indicating strong IRD supply from terrestrial sources, while partly significantly enhanced accumulation rates of rounded quartz particles (~0.015 g cm^{-2} kyr^{-1}) point to a temporally strengthened supply of sea-ice rafted material. Accumulation rates of angular quartz and dark minerals mostly co-vary, while rounded quartz is temporarily anti-correlated to the mineral components mentioned before (Fig. 7).

4.3. Kamchatka IRD assemblage

The co-abundance of dark minerals and angular quartz grains in eastern Okhotsk Sea sediments during late MIS 6, Termination II, and MIS 3 (Fig. 7) is classified here as 'Kamchatka $IRD_{iceberg}$ Assemblage'. Their enhanced accumulation close to Kamchatka is significantly higher than in any other of the five time slices investigated throughout the transect pointing to iceberg supply from Kamchatkan terrestrial sources. In order to better discriminate periods rich in this assemblage from time intervals relatively poor in those two minerals, we compared median values of dark mineral and angular quartz accumulation rates over different time slices (Fig. 8). The increase of angular quartz particularly during Termination I in the westernmost core may be related to the supply of terrestrial IRD from western

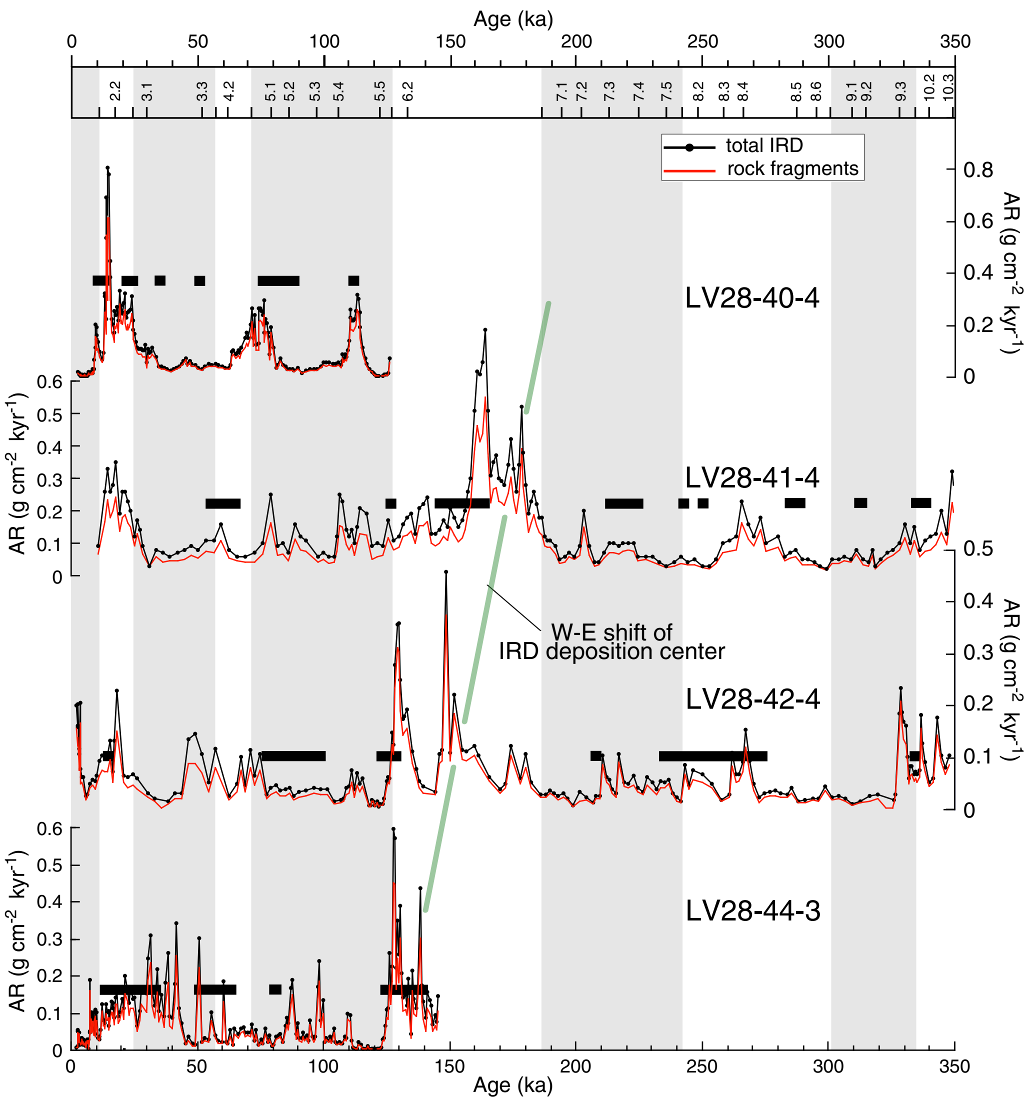

Fig. 5. Accumulation rates of IRD_{total} (bold black line with dots), and accumulation rates of rock fragments (red line). Green oblique line indicates W–E shift of IRD deposition center during MIS 6. Horizontal black bars represent the occurrence of large dropstones. Shaded areas mark interglacial periods.

source areas, while a contribution of eastern sources seems unlikely as dark mineral accumulation rates remain low.

4.4. Oxygen isotope anomalies

Generally, planktonic and benthic isotope records from the central and western Okhotsk Sea (Fig. 2) reveal reasonable agreement to global isotope stacks and well reflect northern hemispheric glacial–interglacial cycles. In contrast, the easternmost Okhotsk Sea planktonic $\delta^{18}O$ record exhibits a rapid isotopic shift of ~1.9‰ across Termination II largely exceeding the normal deglacial $\delta^{18}O$ amplitude of 1.1–1.3‰. In particular during MIS 6.3, 5.5, and 5.4, anomalously light planktonic $\delta^{18}O$ values (Fig. 9) point to temporarily fresher surface conditions in the eastern Okhotsk Sea, most likely due to strong, regional ice melting from Kamchatka.

5. Discussion

The concept of a pervasive East Siberian or Beringian ice sheet covering the regions east and north of the Okhotsk Sea during the LGM (Grosswald, 1998; Grosswald and Hughes, 1998, 2002) was already questioned by Nürnberg et al. (1995), and finally refuted by Gualtieri et al. (2000) and Brigham-Grette et al. (2003). Brigham-Grette et al. (2001) already proved that LGM glaciations on the far eastern Chukotka Peninsula were restricted to some highland areas, and that older Pleistocene ice advances (but younger than MIS 11) extended beyond the modern Russian coastline. Recently, Bigg et al. (2008) proposed two stages of Kamchatka glaciation during the last glacial, with an extensive Kamchatka-Koryak Ice Sheet and marine-terminating ice margins prior to 40 ka BP, and largely reduced, montane-based icefields at 18 ka BP with only few glacier outlets reaching the sea. For the adjacent Okhotsk Sea region we discuss evidence that mainly during MIS 6 and also during MIS 3 parts of SW-Kamchatka were glaciated, and that iceberg-releasing mountain glaciers protruded down to sea level. Based on IRD flux rates and mineral assemblages we highlight the interplay of iceberg transport and sea-ice rafting particularly during these periods, and throughout the past 350 ka.

5.1. Ice rafting and IRD entrainment processes

The accumulation rates of sand-sized ice rafted particles presented in Figs. 5 and 7 indicate that IRD is present in varying abundances in the Okhotsk basin over the past 350 ka. Although highest flux rates

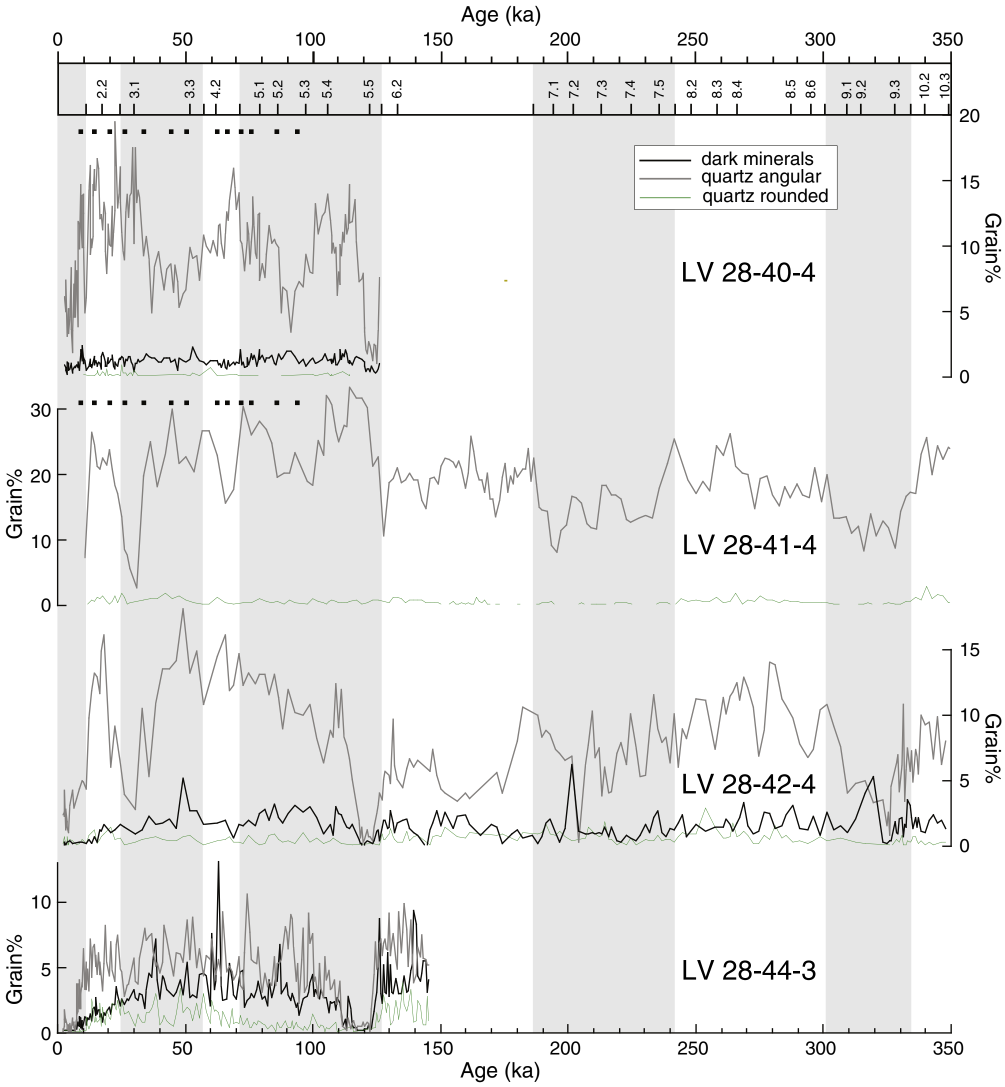

Fig. 6. IRD grain percentages of angular (bold gray line) and rounded quartz (thin green line), and dark minerals (bold black line). Shaded areas mark interglacial periods. Black squares indicate Okhotsk Sea sea-ice expansion events postulated by Sakamoto et al. (2005).

are clearly related to glacial periods, IRD even occurs during interglacial periods. Hence, drifting sea-ice must be regarded as an important basin-wide distributor of coarse-grained lithic material (see Nürnberg and Tiedemann, 2004), as in the modern Okhotsk Sea icebergs are unknown.

While $IRD_{iceberg}$ is rather angular material of terrigenous origin and ruptured from weathered rock outcrops on the earth surface (Krissek and St. John, 2002), $IRD_{sea\text{-}ice}$ is incorporated into newly forming ice from the shallow coastal seabed under cold and stormy conditions, and later again melt-released to the deep-sea (e.g. Reimnitz et al., 1993b; Nürnberg et al., 1994; Eicken et al., 2000; Stierle and Eicken, 2002; Dethleff and Kuhlmann, 2010). Processes like nearshore anchor ice formation, seabed freezing of grounded ice floes, tidal pumping, floe-bulldozing, suspension freezing and beach-ice formation (e.g. Osterkamp and Gosink, 1984; Reimnitz et al., 1987; Rearic et al., 1990; Reimnitz et al., 1993c; Ackermann et al., 1994; Reimnitz et al., 1998) can be favored for the entrainment of both coarse angular and rounded clasts from sand to pebble size into the Okhotsk sea-ice cover.

In first approximation we interpret the co-abundance of rounded and angular coarse quartz grains in Okhotsk Sea deposits as tracer for sea-ice transport, since both particle shapes are most efficiently rafted in turbulent shallow water areas like coastal or shore polynyas (Reimnitz et al., 1987, 1993c; Ackermann et al., 1994; Dethleff, 2005, Dethleff and Kuhlmann, 2010). In the present and past Okhotsk Sea, potential $IRD_{sea\text{-}ice}$ entrainment areas are located on the tidally influenced (Kowalik and Polyakov, 1998) northern, western and eastern shelf areas, providing hydrodynamically reworked coarse clasts through Pleistocene and Holocene times (Svitoch, 2003). The downcore distribution of $IRD_{sea\text{-}ice}$ in deep-sea sediments thus, well reflects spatial and temporal variations of the sea-ice coverage as well as main areas of ice melt and particle release.

Only during extreme glacial conditions with extended terrestrial glaciation, the supply of $IRD_{iceberg}$ provided by calving glaciers may have prevailed. The stratigraphic abundance of $IRD_{iceberg}$ in Okhotsk Sea deposits can thus be used as tracer for iceberg ablation areas in the marine environment, for the identification of iceberg drift pathways and, finally, for the reconstruction of ice sheet advance on adjacent landmasses down to sea level.

5.2. Ice rafting and cryogenesis during glacials

Nürnberg and Tiedemann (2004) provided the longest IRD record from the central Okhotsk Sea so far covering 1.1 Ma (MIS 32). Their

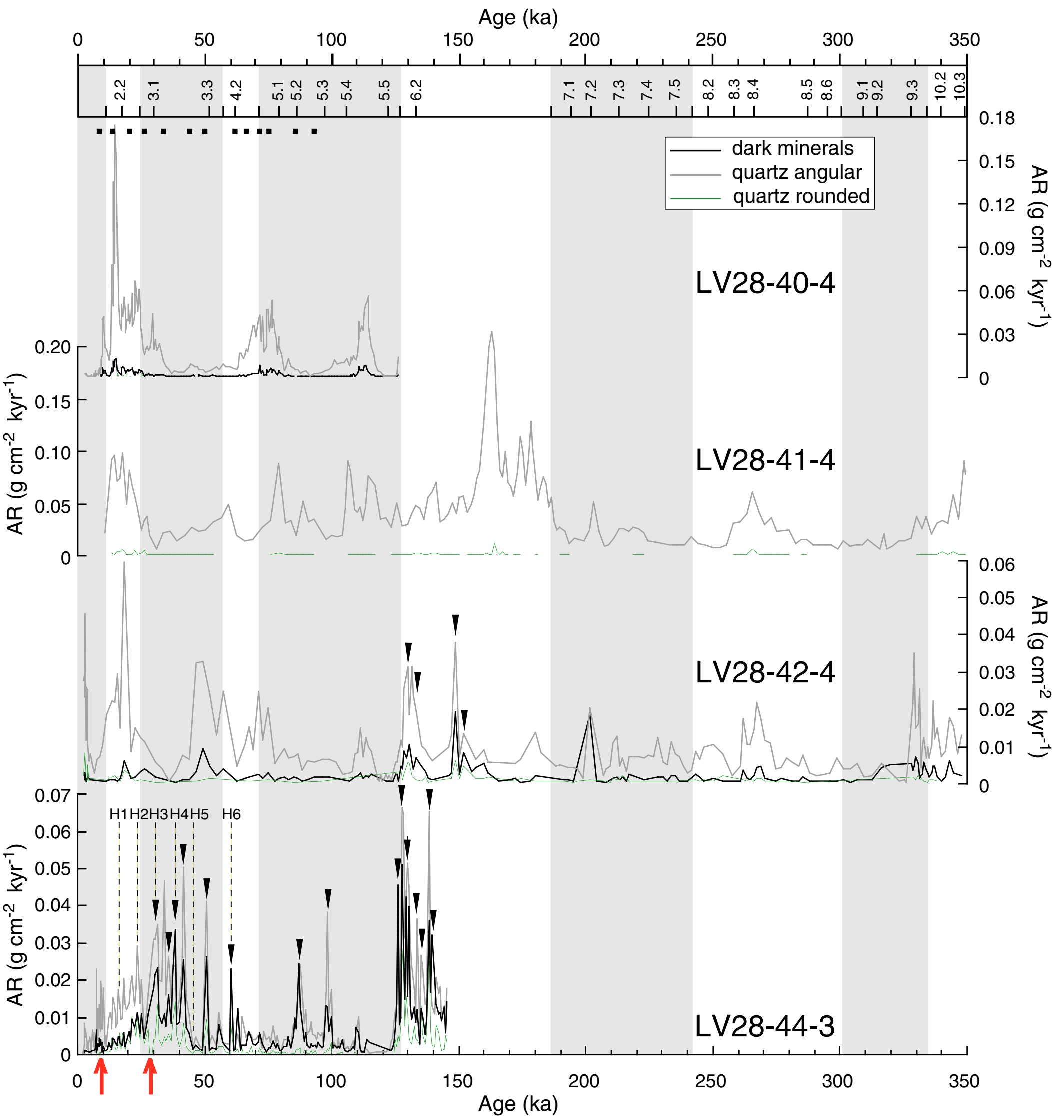

Fig. 7. Accumulation rates of angular (gray line) and rounded quartz (thin green line), and dark minerals (black line). Black triangles indicate periods of co-abundances of dark minerals and angular quartz, pointing to iceberg transport from W-Kamchatka. The $IRD_{iceberg}$ events during MIS 6.2, Termination II, MIS 3, and very distinctly at MIS 5.4 and 5.2 cold events are accompanied by strong sea-ice rafting indicated by enhanced flux rates of rounded quartz. Heinrich events (H1 to H6) are marked for comparison (stippled lines). Red arrows indicate volcanic ash layers found in core LV28-44-3. Shaded areas mark interglacial periods. Black squares indicate Okhotsk Sea sea-ice expansion events postulated by Sakamoto et al. (2005).

data records imply extensive sea ice coverage during glacials, promoted by a strong Siberian high pressure cell, which interacts with the Aleutian low pressure system. The late glacial/deglacial maxima in IRD flux are synchronous and succeeded by high marine productivity events. Marine productivity strengthened due to the effective nutrient utilization at times of an enhanced water column stratification and high nutrient supply from fluvial river-runoff and sea ice thawing.

Figs. 5 and 7 show that since MIS 10 the IRD fluxes at sites LV28-41-4 and LV28-42-4 were largely synchronous to the hemispheric glacial–interglacial changes. During full glacial conditions (MIS 10, 8, and 4), we propose a seasonal to temporarily perennial, but mobile and highly dynamic sea-ice cover extending from northern, western and eastern shores far south, waxing and waning frequently over the central transect cores as indicated by enhanced IRD (but not as extremely high as in MIS 6 and MIS 2 as will be discussed below) dispersed by freely floating sea-ice. Shore rafting was the prevailing process for IRD supply, and marine productivity was generally low (Nürnberg and Tiedemann, 2004). Toward the end of both MIS 10 and 8, the increasing abundance and diversity of microfossils point to climatic warming and related deteriorating sea-ice cover and open water (e.g., Barash et al., 2006; Wang and Wang, 2008).

For MIS 4 and 2, Wang and Wang (2008) proposed largely expanded and perennial Okhotsk Sea ice coverage. Our findings support and refine this assumption. During mid MIS 2, the partly extremely high IRD accumulation rates in the two westernmost cores (Figs. 5, 7) may be exclusively explained by seasonal to year-round $IRD_{sea\text{-}ice}$ supply from western and northwestern Okhotsk Sea shelves. This assumption is supported by low biomarker concentrations pointing to a significantly reduced marine productivity (Ternois et al., 2001). No indications are available for iceberg supply. The western situation is contrasted by lower – and toward Termination I further decreasing – IRD fluxes in the core closest to Kamchatka, which clearly points to a rather seasonal ice coverage with pronounced periods of summer open water in the eastern part of the Okhotsk Sea.

For deglacial Termination I (~15–7 ka BP) we postulate a further retreating seasonal sea-ice coverage with increasing periods of open water in the eastern Okhotsk Sea (decreasing IRD, increasing benthic foraminifer fluxes at site LV28-44-3), which is in agreement to the micropaleontological and sedimentological findings of Shiga and

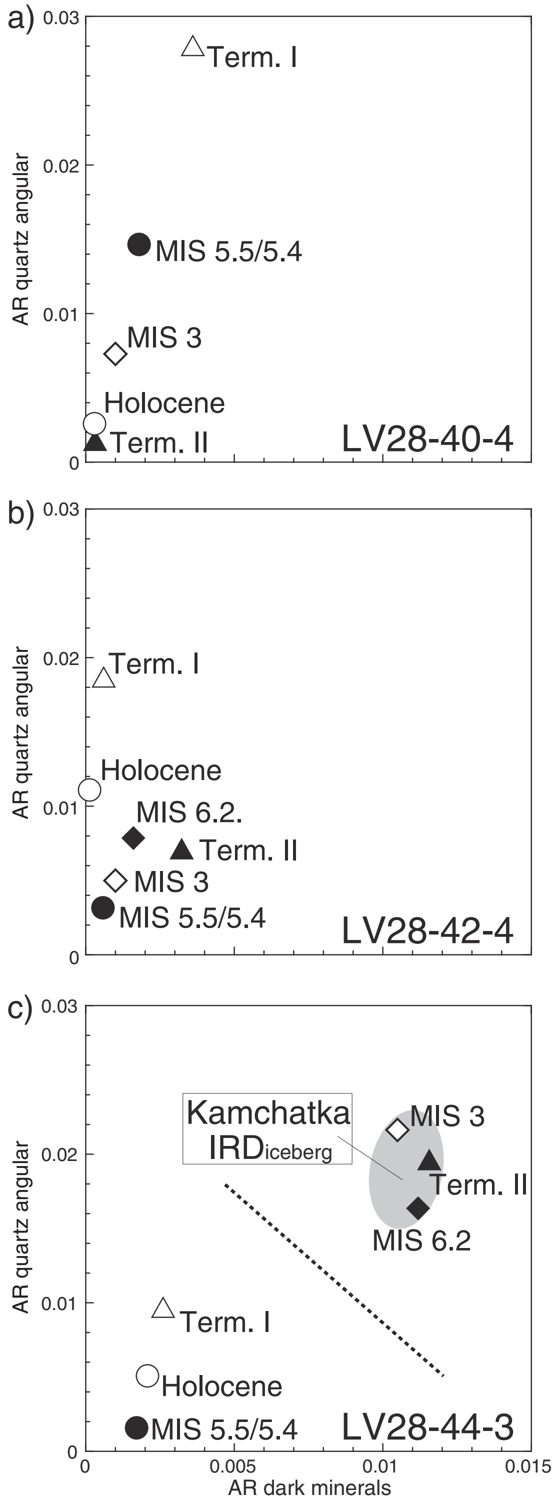

Fig. 8. Median accumulation rates (in g cm^{-2} kyr^{-1}) of angular quartz *versus* dark minerals, differentiated for various time slices: MIS 6.2 (~143.5–136.0 ka, black squares), Termination II (~129.3–123.0 ka, black triangles), MIS 5.5/5.4 (122.0–106.0 ka, black dots), MIS 3 (~45–30 ka, open squares) Termination I (15.5–7.3 ka, open triangles), and the Holocene (~11.0–0 ka, open circles). a) core LV28-40-4 western Okhotsk Sea, b) core LV28-42-4 central Okhotsk Sea, and c) core LV28-44-3 eastern Okhotsk Sea. Core LV28-41-4 is not presented as it lacks dark minerals. Note the extraordinarily high accumulations rates of dark minerals and angular quartz in the eastern Okhotsk Sea during MIS 6, Termination II, and MIS 3.

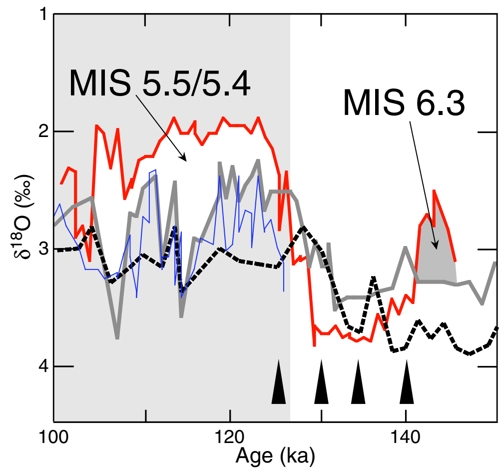

Fig. 9. Planktonic $\delta^{18}O$ records across the Okhotsk Sea. The easternmost core LV28-44-3 shows prominent $\delta^{18}O$ deviations (red line) during late MIS 6 and early MIS 5 related to freshwater supply in contrast to cores LV28-40-4 (blue line), LV28-41-4 (dashed line), and LV28-42-4 (gray line). Black triangles indicate major $IRD_{iceberg}$ events. Shaded area marks interglacial periods.

Koizumi (2000), Okazaki et al. (2003) and Wang and Wang (2008). For the western Okhotsk Sea, we can also trace a retreating seasonal sea-ice coverage with increasing periods of open water from lowering IRD fluxes, which is congruent to Shiga and Koizumi (2000). Our postulated decrease of the seasonal ice cover in the entire Okhotsk Sea is further supported by Gorbarenko (1996) and Ternois et al. (2001), who pinpointed increasingly warmer summer conditions and related enhanced nutrient supply during the last deglacial period based on IRD and biomarker studies.

5.3. Interglacial ice rafting

Analogous to today's summer situation of a pronounced Mongolian Heat Low and a strong Hawaiian High, we assume prevailing SE monsoonal winds during interglacials. High marine productivity (although being lower than during deglaciations) is favored by the strong freshwater discharge induced by high precipitation rates in the Amur drainage area and by a seasonally reduced and mobile sea-ice cover (Nürnberg and Tiedemann, 2004) with lower waxing/waning frequency over the central transect part as indicated by lowered IRD flux rates.

In particular during MIS 5.5 and MIS 5.4 (Fig. 10), extremely low IRD accumulation rates at core sites LV28-42-4 and LV28-44-3 suggest nearly permanent open water conditions with only sporadic winter ice-sediment transport in the eastern Okhotsk Sea. This finding is supported by enhanced flux rates of benthic foraminifers (Fig. 11) and diatom abundances (Wang and Wang, 2008) indicating significantly enhanced marine productivity. Deduced from the decreasing IRD fluxes from core LV28-40-4 toward core LV28-41-4, we suggest a limited seasonal ice coverage for the western Okhotsk Sea with clearly decreasing ice density further east.

During the Holocene Climatic Optimum (~6 ka BP) we infer nearly permanent ice-free conditions in the entire Okhotsk Sea with sporadic winter ice formation and particle supply from the extremely low IRD fluxes at core sites LV28-40-4, LV28-42-4 and LV28-44-3, being congruent to Shiga and Koizumi (2000) and Sakamoto et al. (2003). Wang and Wang (2008) also proposed only seasonal sea ice conditions for that interval deduced from higher proportions of high-productivity diatom assemblages and increasing numbers of valves. After the Holocene Climatic Optimum, the Okhotsk Sea ice conditions developed toward modern conditions.

The 13 Okhotsk Sea sea-ice events (OSIE) postulated by Sakamoto et al. (2005) for the last 100 kyr in the western Okhotsk Sea (Figs. 6 and 7) are neither reflected consistently in our grain percentages nor in the IRD accumulation rates. Many of the millennial-scale sea-ice

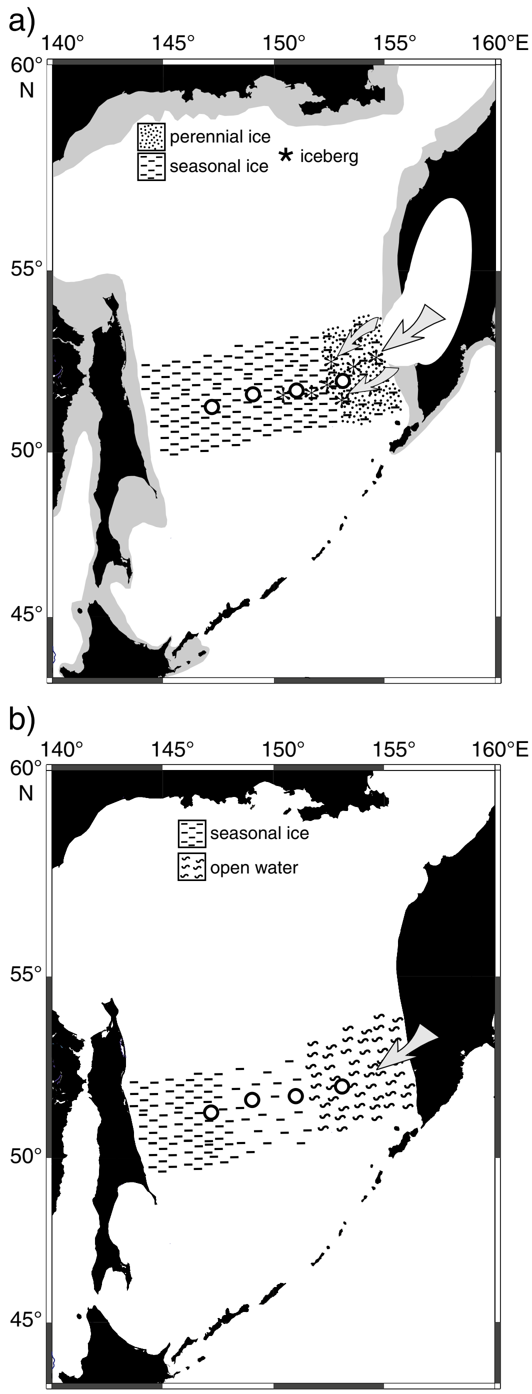

Fig. 10. Sketches of paleo-cryological development in the Okhotsk Sea contrasting a) full glacial heavy ice conditions along the core transect during late MIS 6 and Termination II, and b) rather ice-reduced to ice free conditions during early MIS 5.5/5.4. White area on SW-Kamchatka schematically indicates the postulated extended mountain glaciation, while arrows indicate direction of glacier protruding, iceberg drift, and melt water streams, respectively. Gray shaded off-coastal band in a) indicates exposed shelf areas due to glacially lowered sea level.

advances are in fact characterized by low IRD grain percentages and low IRD accumulation rates in our cores, in particular during MIS3 and MIS 5.

5.4. Extreme glacial MIS 6 ice conditions

5.4.1. Shift of IRD deposition center — Reflection of changing ice conditions

The general increase of IRD accumulation rates during MIS 6 in all cores (Figs. 5, 7; except LV28-40-4) points to intensified particle

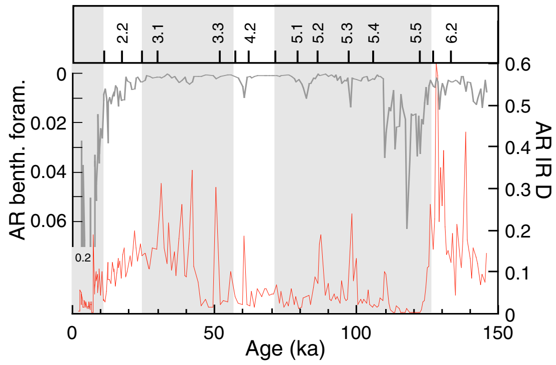

Fig. 11. Comparison of IRD_{total} accumulation rates (in g cm^{-2} kyr^{-1}, red curve) and accumulation rates of benthic foraminifers (in g cm^{-2} kyr^{-1}, inversed, gray curve) at the easternmost sediment core LV28-44-3 off Kamchatka. Flux data were calculated from foraminifer percentages taken from Kaiser (2000). Shaded areas mark uneven MIS.

transport by ice. Over a period of ~40 kyr, the IRD deposition center shifted from the western Okhotsk Sea (early MIS 6) toward Kamchatka (late MIS 6) marked by the temporal and spatial progression of the accumulation rate peaks (Fig. 5). We suppose that during early and mid MIS 6 the ice cover was seasonal to year-round and mobile (high IRD supply) in the western, but rather of seasonal and patchy development (low IRD supply) in the eastern Okhotsk Sea. During late MIS 6, this situation changed toward a seasonal to perennial, but still mobile ice cover (high IRD supply) in the eastern Okhotsk Sea dominated by drifting icebergs and related particle-supply from Kamchatka as will be shown below, and to a rather seasonal ice coverage in the western sea supplying less IRD (Fig. 10). This MIS 6 ice scenario is supported by Wang and Wang (2008), who identified an almost entirely ice-covered central Okhotsk Sea during that period based on rare occurrences of diatoms and increasing sea-ice assemblages.

5.4.2. Icebergs vs. sea-ice

Analogous to the modern winter situation, we assume that during full glacial times – particularly like MIS 6 – a strong Siberian High and a pronounced Aleutian Low persisted (Nürnberg and Tiedemann, 2004). Such a constellation of atmospheric pressure cells caused predominant northerly (offshore) winds in the Okhotsk Sea area promoting sea-ice formation and related rafting processes in coastal polynyas. The particle-laden sea-ice was transported offshore by winds and tidal currents, and – in periods of modern-like sea level – also by the anti-cyclonal surface current system. During the short glacial summer, the lithic freight was released from the sea-ice, and contributed to deep-sea sedimentation. Significantly enhanced values of IRD_{total} and the transect-wide abundance of dropstones during MIS 6 and Termination II, indeed, point to a basin-wide, seasonal to perennial – but continuously dynamic and mobile – ice coverage.

However, the varying roundness of dropstones and consistently high flux rates of terrestrial rock fragments imply both sea-ice transport and iceberg supply. To differentiate between $IRD_{iceberg}$ and $IRD_{sea\text{-}ice}$ supply to Okhotsk Sea sediments, and thus, to trace glacier-related iceberg dispersal and sea-ice rafting particularly during late MIS 6 in detail, we focus on the downcore distribution of generally less abundant, but temporally and spatially extremely varying IRD components like terrestrial dark minerals in combination with angular and rounded quartz grains (Fig. 7).

Significantly enhanced concentrations of dark minerals associated with outstanding high abundances of angular quartz grains in the eastern cores (Fig. 7) are attributed to iceberg supply from Kamchatka. According to the geographical, geological and petrographic settings, most likely sources of enhanced dark mineral and angular quartz supply to eastern Okhotsk deep-sea deposits ('Kamchatka $IRD_{iceberg}$ Assemblage') are located in the Sredinny Mountain Range on southwestern Kamchatka (Figs. 1, 10) consisting of amphibolite-grade paragneisses, metavolcanic rocks and allochthonous metasediments (Bindemann et al., 2002), and in adjacent volcanic provinces. Temporal variations in the 'Kamchatka $IRD_{iceberg}$ Assemblage' are thus related to expansion down to sea level and shrinking of montane glaciers on the adjacent source mainland, respectively (Kent et al., 1971; Dunhill and Reimnitz, 2000; Krissek and St. John, 2002).

The notion of late MIS 6 Kamchatka iceberg supply to the eastern Okhotsk Sea is strongly supported by a change of the regional IRD composition toward high flux rates of terrestrial dark minerals and angular quartz particularly in core LV28-44-3 (Fig. 7). Coinciding with the W–E shift of the IRD_{total} deposition center, the Kamchatka-slope core reveals strong variations in flux-rates as well as in co-abundance of dark minerals and angular quartz on millennial timescales (Fig. 7), which suggest rapid changes in IRD supply by icebergs. Interestingly, nearly identical sequences of co-abundance of dark mineral and angular quartz flux rates are evident during the period from late MIS 6 and during Termination II, pointing to comparable ice mobility and $IRD_{iceberg}$ transport processes (Fig. 12).

Our data point to temporarily enhanced supply of terrestrial lithic material through icebergs, accompanied by strong sea-ice rafting indicated by coinciding enhanced flux rates of rounded quartz grains at ~138 ka, ~135 ka, ~129 ka, and ~128 ka BP (Figs. 7, 12). During the remaining time, sea-ice transport was reduced as indicated by lowered rounded quartz supply, while iceberg supply remained strong (in particular at ~140 ka, ~134 ka, ~130 ka, and ~126 ka BP). Terrestrial findings provide further evidence for major Kamchatka glaciations during the past. According to Braitseva and Melekestsev (1974) and Ananjev et al. (1984), the northern and eastern coastal regions of the Okhotsk Sea as well as Kamchatka were partly glaciated in former times. During mid-Pleistocene times, mountain glaciers of predominantly alpine character (Arkhipov et al., 1986) most probably reached down to sea level along the western Kamchatka coast as testified by extended moraines (Zech et al., 1996, 1997) and dating of local near-shore glacial deposits (Bäumler and Zech, 2000).

We suppose that during late MIS 6 and early Termination II the offshore drift of icebergs from the western coast of Kamchatka toward the open sea (Fig. 12) required several regional prerequisites: i) prevalence of strong and continuous offshore glacier winds (iceberg drag), ii) weakening of the northbound West Kamchatka Current in line with a lowered sea level and the diminished gyre-feeding water mass inflow from the adjacent sub Arctic North Pacific Ocean and, iii) a highly mobile or even slightly reduced coastal sea-ice cover. The latter assumption fits well to the lowered fluxes of rounded quartz particles at specific times.

5.4.3. Isotopic offset and freshwater supply

Planktonic oxygen isotope records (Fig. 2) provide further evidence for Okhotsk Sea ice conditions and Kamchatka glaciation. We suggest that the anomalously light $\delta^{18}O$ values during MIS 6.3 at the easternmost site LV28-44-3 (Fig. 9), accompanied by low IRD_{total} but enhanced benthic foraminiferal fluxes (Fig. 11), point to rather ice-free

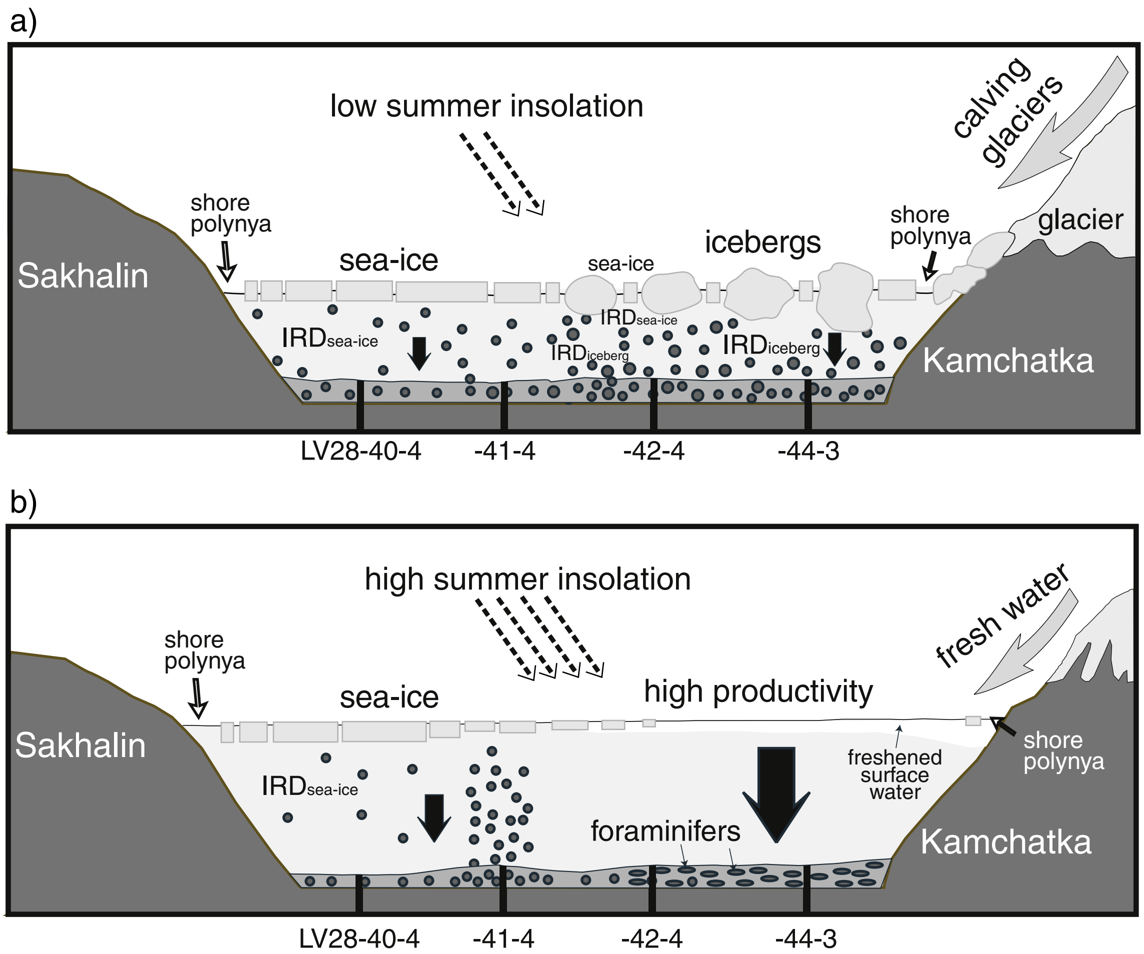

Fig. 12. Schematic cross-section of the Okhotsk Sea basin showing the cryological and oceanographic conditions during late MIS 6 and Termination II (upper diagram), and from MIS 5.5 to MIS 5.4 (lower diagram).

conditions in the eastern Okhotsk Sea at times of a generally more complex, more extensive, and longer lasting glaciation in northern Russia and Siberia compared to subsequent glaciations (Svendsen et al., 2004). Ice-free conditions might have been favored by the presence of the northbound West Kamchatka Current, transferring W-Pacific water masses along the W-Kamchatka continental margin. It might be speculated that strengthened evaporation in ocean areas influenced by the West Kamtchatka Current and subsequent precipitation over Kamchatka strengthened ice sheet growth with mountain glaciers expanding gradually down to sea level.

After MIS 6.3, the Kamchatka Current inflow diminished, sea ice conditions strengthened indicated by a rapidly increasing $IRD_{sea\text{-}ice}$ accumulation and a clearly reduced benthic foraminiferal flux, and iceberg calving causing regional $IRD_{iceberg}$ dispersal and deposition commenced (Figs. 11, 12). The younger, extended and even more pronounced $\delta^{18}O$ offset between western and eastern core locations at interglacial MIS 5.5 and MIS 5.4 may rather be related to a long-term freshening attributed to the ice-sheet retreat on Kamchatka peninsula coincident with global warming and the strengthening of the West Kamchatka Current. At that time, the accumulation of IRD_{total} (including dark minerals) ceased, and benthic foraminiferal fluxes increased in the eastern Okhotsk Sea (Fig. 11) indicating little or even no ice cover from MIS 5.5 to 5.4.

5.5. Extraordinary MIS 3

Bigg et al. (2008) discussed the extent of the Last Glacial glaciation in Eastern Asia. They postulated a significant increase in iceberg flux in the NW Pacific at ~41–36 ka BP, preceding and accompanying a prominent volcanic ash deposit identified in the NW Pacific ODP Site 883. The authors speculated that the collapse of their postulated Kamchatka-Koryak ice-sheet triggered substantial volcanic activity, which in turn might have favored ice sheet decay.

In our sediment core LV28-44-3 closest to Kamchatka, both high IRD_{total} and dark mineral accumulation rates showing millennial-scale variations and the close correlation between dark minerals and angular quartz suggest rapid and enhanced iceberg discharge from Kamchatka during ~45–30 ka BP, although with lesser amplitude variations and commonly lower flux rates as observed for MIS 6 (Figs. 5, 7). Notably, our data records postulate $IRD_{iceberg}$ deposition at ~60 ka, ~51 ka, ~42 ka, ~38 ka, ~36 ka, and ~31 ka, which partly correspond to N-Atlantic Heinrich Events H6, H4, H3, and H2. As not all Heinrich Events (H5 and H1) are represented in our records and due to the stratigraphic constraints, we hesitate to assume a mechanistic coupling between N-Atlantic iceberg armadas and sealevel-reaching Kamchatkan mountain glaciers and related iceberg discharges. Also, as we do not observe a convincing correlation between the Kamchatkan iceberg discharge events and volcanic ashes found in the same core at ~29 ka (although this is closely following the ~31 ka iceberg discharge event), and at ~9 ka, our data are not able to support the Bigg et al. (2008) hypothesis of intensified volcanism during phases of Kamchatka ice sheet decay.

6. Conclusions

IRD and $\delta^{18}O$ data records from a W–E-trending sediment core transect across the central Okhotsk Sea provide insight into the late Pleistocene glaciomarine depositional history and hence, the paleo-cryological development of the Okhotsk Sea. The following conclusions can be drawn:

1) Ice-rafted debris is abundant in varying concentrations throughout the last ~350 ka. The component analyses of ice-rafted material allowed to differentiate between material supplied by sea-ice ($IRD_{sea\text{-}ice}$) from that transported by icebergs originating from adjacent glaciated land regions ($IRD_{iceberg}$).
2) IRD deposition in the central Okhotsk Sea is characterized by rather synchronous basinwide IRD supply over glacial–interglacial cycles. Lowered particle accumulation rates relate to warm interglacial periods with reduced and seasonal sea-ice coverage (e.g. MIS 5.5–5.4, Holocene Climatic Optimum), while high IRD supply reflects glacial times with more extended and dynamic ice covers. Long-term IRD fluxes are on average higher in western Okhotsk Sea sediment records than in the central and eastern part, pointing to a more continuous particle-supplying sea-ice cover through time.
3) MIS 6 is different to other glacials with respect to IRD deposition. In all our sediment cores the IRD accumulation rates were higher by factor 2–3 during MIS 6 and exceeded the particle fluxes during the remaining isotope stages by a factor of 3 to 10. Notably, the IRD deposition center shifted from the western Okhotsk Sea (early MIS 6) toward Kamchatka (late MIS 6) indicating asynchronous IRD accumulation. For early to mid MIS 6, the western Okhotsk Sea sea-ice cover was seasonal to perennial supplying high IRD rates, while the eastern ice cover was rather patchy causing low IRD fluxes. Toward late MIS 6, instead, the eastern sea-ice cover became seasonal to perennial, although remaining highly mobile, coinciding with strong Kamchatka iceberg-dispersal. The western Okhotsk Sea ice coverage tended to remain seasonal receiving lesser IRD portions.
4) During late MIS 6, the eastern Okhotsk Sea IRD composition was characterized by dark minerals, typically hornblende and pyroxene. Both, the characteristic composition of IRD and the significantly enhanced accumulation rates of dark minerals and angular quartz let us argue that the IRD originates from distinct source areas on Kamchatka and was dispersed by icebergs across the eastern Okhotsk Sea ($IRD_{iceberg}$). This scenario affords at least the presence of extended mountain glaciers at that time protruding down to sea level on the western side of Kamchatka. Substantial prerequisites for off-coastal iceberg drift from Kamchatka were strong offshore glacier winds, a flexible ice cover, and a weakened West Kamchatka Current.
5) Anomalously light planktonic stable oxygen isotopes in core LV28-44-3 during MIS 6.3, late Termination II and MIS 5.5–5.4 imply significant freshwater contribution to the eastern Okhotsk Sea providing evidence for postglacial melting of Kamchatkan icebergs and glaciers. From extremely low IRD accumulation rates during MIS 5.5 and MIS 5.4, we assume nearly permanent open water conditions with only sporadic winter ice-sediment transport in the eastern Okhotsk Sea.
6) The intensified Kamchatka glaciation during MIS 6 represented in our easternmost cores LV28-44-3 and LV28-42-4 was repeated during MIS 3 with comparable intensity. $IRD_{iceberg}$ events were dated to ~60 ka, ~51 ka, ~42 ka, ~38 ka, ~36 ka, and ~31 ka, and partly correspond to N-Atlantic Heinrich Events. These events are not seen further to the west. Here, partly extremely high IRD accumulation during MIS 4 and 2 indicates seasonal to perennial IRD supply, associated with a partly permanent but mobile ice cover.
7) During Termination I, we propose a retreating seasonal sea-ice cover with increasingly open water conditions in the eastern Okhotsk Sea. During the Holocene Climatic Optimum, we presume nearly perennially ice-free conditions in the entire Okhotsk Sea with only sporadic winter ice formation and IRD supply.
8) Our sedimentological and isotope geochemical data do not support the notion that during the last 350 ka Kamchatka was covered by an extensive ice cap, as postulated by others. Enhanced iceberg discharge from Kamchatka as deduced for late MIS 6, Termination II, and MIS 3 can to our mind be explained by the expansion of montane glaciers down to sea level.

Acknowledgments

Funding of this research contribution was provided by the German Science Foundation (DFG) and by the Ministry of Science and

Technology (BMBF). We thank the Russian crew and the Shipboard Scientific Party of RV Akademik Lavrentiev cruise 28 (1998), which took place in the framework of the joint German/Russian project "KOMEX". Large parts of the data sets were assembled in the framework of the Ph.D. thesis of AK. AMS^{14}C measurements were kindly provided by the Leibniz Laboratory for Radiometric Dating and Isotope Research, Kiel University.

Appendix A. Supplementary data

Supplementary data to this article can be found online at doi:10.1016/j.palaeo.2011.07.011.

References

Ackermann, N.L., Shen, H.T., Sanders, B., 1994. Experimental studies of sediment enrichment of Arctic ice covers due to wave action and frazil entrainment. J. Geophys. Res. 99 (C4), 7761–7770.
Alfutis, M.A., Martin, S., 1987. Satellite passive microwave studies of the Sea of Okhotsk ice cover and its relation to oceanic processes, 1978–1982. J. Geophys. Res. 92 (C12), 13,013–13,209.
Ananjev, G.S., Ananjeva, E.G., Pakhomov, A.J., 1984. Quaternary glaciation of the east Priokhotja. In: Bespaluj, V.G. (Ed.), Pleistocene Glaciation of the Eastern Asia: Far Eastern Branch of Akademy Nauk of the SSSR, Magadan, pp. 43–56.
Arkhipov, S.A., Bespaly, V.G., Faustova, M.A., Glushkova, O.Yu., Isaeva, L.L., Velichko, A.A., 1986. Ice sheet reconstruction. Quaternary Glaciations in the Northern Hemisphere: Quat. Sci. Rev. 5, pp. 475–483.
Barash, M.S., Matul, A.G., Kazarina, G.Kh., Khusid, T.A., Abelmann, A., Biebow, N., Nürnberg, D., Tiedemann, R., 2006. Paleoceanography of the central Sea of Okhotsk during the Middle Pleistocene (350–190 ka) as inferred from micropaleontological data. Oceanology 46 (4), 501–512.
Bassinot, F.C., Labeyrie, L.D., Vincent, E., Quidelleur, X., Shackleton, N.J., Lancelot, Y., 1994. The astronomical theory of climate and the age of the Brunshes-Matuyama magnetic reversal. Earth Planet. Sci. Lett. 126, 91–108.
Bäumler, R., Zech, W., 2000. Quaternary paleosols, tephra deposits and landscape history in South Kamchatka, Russia. Catena 41, 199–225.
Biebow, N., Hütten, E., 1999. KOMEX cruise reports: KOMEX I and II: RV Professor Gagarinsky Cruise 22, RV Akademik M.A. Lavrentyev Cruise 28, GEOMAR Report 82.
Bigg, G.R., Clark, C.D., Hughes, A.L.C., 2008. A last glacial ice sheet on the Pacific Russian coast and catastrophic change arising from coupled ice-volcanic interaction. Earth Planet. Sci. Lett. 265, 559–570. doi:10.1016/j.epsl.2007.10.052.
Bindemann, I.N., Vinogradov, V.I., Valley, J.W., Wooden, J.W., Natal'in, B.A., 2002. Archean protolith and accretion of crust in Kamchatka: SHRIMP dating of Zirkon from Sredinny and Ganal Massifs. J. Geol. 110, 271–289.
Braitseva, O.A., Melekestsev, I.V., 1974. Quaternary glaciation. In: Luchitskiy, I.B. (Ed.), Kamchatka, Kurile and Komandor Islands. Nauka, Moscow, pp. 426–438.
Brigham-Grette, J., Hopkins, D.M., Ivanov, V.F., Basilyan, A., Benson, S.L., Heiser, P.A., Pushkar, V., 2001. Last interglacial (isotope stage 5) glacial and sea level history of coastal Chukotka Peninsula and St. Lawrence Island, western Beringia. Quat. Sci. Rev. 20 (1–3), 419–436.
Brigham-Grette, J., Gualtieri, L.M., Glushkova, O.Yu., Hamilton, T.D., Mostoller, D., Kotov, A., 2003. Chlorine-36 and ^{14}C chronology support a limited last glacial maximum across central Chukotka, northeastern Siberia, and no Beringian ice sheet. Quat. Res. 59, 386–398.
Darby, D.A., 2003. Sources of sediment found in sea ice from the western Arctic Ocean, new insights into processes of entrainment and drift patterns. J. Geophys. Res. 108 (C8), 3257. doi:10.1029/2002JC001350.
Dethleff, D., 2005. Entrainment and export of Laptev Sea ice sediments, Siberian Arctic. J. Geophys. Res. 110 (C7), C07009. doi:10.1029/2004JC002740.
Dethleff, D., Kuhlmann, G., 2010. Fram Strait sea ice sediment provinces based on silt and clay compositions identify Siberian Kara and Laptev Sea as main source regions. Polar Res. doi:10.1111/j.1751-8369.2010.00149.x.
Dethleff, D., Rachold, V., Tintelnot, M., Antonov, M., 2000. Sea-ice transport of riverine particles from the Laptev Sea to Fram Strait based on clay mineral studies. Int. J. Earth Sci. 89, 496–502.
Dunhill, G., Reimnitz, E., 2000. Comparison of sea-ice sediment to iceberg rafted debris: grain size, surface features and grain shape. Program and Abstracts of The 30th International Arctic Workshop. Institute of Arctic and Alpine Research, Boulder, Colorado, p. 54.
Eicken, H., Kolatschek, J., Freitag, J., Lindemann, F., Kassens, H., Dmitrenko, I., 2000. A key source area and constraints on entrainment for basin-scale sediment transport by Artic sea ice. Geophys. Res. Lett. 27 (13), 1919–1922.
Frenzel, B., Pesci, M., Velichko, A.A., 1992. Atlas of Paleoclimate and Paleoenvironments of the Northern Hemisphere: Late Pleistocene–Holocene. Gustav Fischer Verlag, Stuttgart, Jena, New York.
Gladyshev, S., Martin, S., Riser, S., Figurkin, A., 2000. Dense water production on the northern Okhotsk shelves: comparison of ship-based spring–summer observations for 1996 and 1997 with satellite observations. J. Geophys. Res. 105 (C11), 26,281–26,299.
Gladyshev, S., Talley, L., Kantakov, G., Khen, G., Wakatsuchi, M., 2003. Distribution, formation, and seasonal variability of Okhotsk Sea Mode Water. J. Geophys. Res. 108 (C6), 3186. doi:10.1029/2001JC000877.
Gloersen, P., Campbell, W.J., Cavalieri, D.J., Comiso, J.C., Parkinson, C.L., Zwally, H.J., 1992. Arctic and Antarctic sea ice, 1978–1987: satellite passive-microwave observations and analysis. Scientific and Technical Information Program, NASA SP-511.
Gorbarenko, S.A., 1996. Stable isotope and lithologic evidence of late-glacial and Holocene oceanography of the northwestern Pacific and its marginal seas. Quat. Res. 46, 230–250.
Gorbarenko, S.A., Derkachev, A.N., Astakhov, A.S., Sauton, J.R., Nürnberg, D., Shapovalov-Chuprynin, V.V., 2000. Lithostratigraphy and tephrachronology of the Upper Quaternary deposits in the Sea of Okhotsk. Geol. Pacif. Ocean. 19 (2), 58–82.
Gorbarenko, S.A., Nürnberg, D., Derkachev, A.N., Astakhov, A.S., Southon, J.R., Kaiser, A., 2002. Magnetostratigraphy and tephrachronology of the Upper Quaternary sediments in the Okhotsk Sea: implication of terrigenous, volcanogenic and biotic matter supply. Mar. Geol. 183, 107–129.
Grosswald, M.K., 1998. Late Weichselian ice sheets in Arctic and Pacific Siberia. Quat. Int. 45/46, 3–18.
Grosswald, M.K., Hughes, T., 1998. Evidence for Quaternary glaciation of the Sea of Okhotsk. In: Horie, S. (Ed.), International Project on Paleoclimatology and Late Cenozoic Climate (IPPCLE) News Letter, 11, pp. 3–11.
Grosswald, M.K., Hughes, T., 2002. The Russian component of an Arctic ice sheet during the Last Glacial Maximum. Quat. Sci. Rev. 21, 121–146.
Gualtieri, L., Glushkova, O., Brigham-Grette, J., 2000. Evidence for restricted ice extent during the last glacial maximum in the Koryak Mountains pf Chukotka, far eastern Russia. GSA Bull. 112 (7), 1106–1118.
Hebbeln, D., 2000. Flux of ice-rafted detritus from sea ice in the Fram Strait. Deep Sea Res., Part II 47, 1773–1790.
Hewitt, A.T., McDonald, D., Bornhold, B.D., 1997. Ice-rafted debris in the North Pacific and correlation to North Atlantic climatic events. Geophys. Res. Lett. 24 (24), 3261–3264.
Kaiser, A., 2000. Ozeanographie, Produktivität und Meereisverbreitung im Ochotskischen Meer während der letzten ca. 350 ka. Ph.D. Thesis, Univ. Kiel. (in German).
Kempema, E.W., Reimnitz, E., Barnes, P.W., 1989. Sea ice entrainment and rafting in the Arctic. J. Sediment. Petrol. 59 (2), 308–317.
Kent, D., Opdyke, N.D., Ewing, M., 1971. Climate change in the North Pacific using ice-rafted detritus as a climatic indicator. Geol. Soc. Am. Bull. 82, 2741–2754.
Kowalik, Z., Polyakov, I., 1998. Tides in the Sea of Okhotsk. J. Phys. Oceanogr. 28 (7), 1389–1409.
Krissek, L.A., St. John, K.E.K., 2002. Pleistocene iceberg production from East Greenland: synchronous between source areas, but distinct from global ice volume. Bull. Geol. Soc. Denmark 49, 79–89.
Leonov, A.K., 1960. The Sea of Okhotsk. NTIS AD 639 585, Nat. Tech. Inf. Serv., Springfield, VA. . 95 pp.
Liu, Y.-J., Song, S.-R., Lee, T.-Q., Lee, M.-Y., Chen, Y.-L., Chen, H.-F., 2006. Mineralogical and geochemical changes in the sediments of the Okhotsk Sea during deglacial periods in the past 500 kyrs. Glob. Planet. Chang. 53, 47–57.
Martin, S., Drucker, R., Yamashita, K., 1998. The production of ice and dense water in the Okhotsk Sea polynyas. J. Geophys. Res. 103 (C12), 27,771–27,782.
Moroshkin, K.V., 1966. Vodnye massy Okhotskogo moray. Nauka, Moscow, 66 pages (English translation: Water masses of the Sea of Okhotsk, NTIS AS J PRS 43942, Natl. Tech. Inf. Serv., Springfield, VA, 1968).
Ninkovitch, D., Opdyke, N.D., Heezen, B.C., Foster, J., 1966. Paleomagnetic stratigraphy, rates of deposition and tephrachronology in North Pacific deep-sea sediments. Earth Planet. Sci. Lett. 1, 476–492.
Nürnberg, D., Tiedemann, R., 2004. Environmental change in the Sea of Okhotsk during the last 1.1 million years. Paleoceanography 19. doi:10.1029/2004PA001023.
Nürnberg, D., Wollenburg, I., Dethleff, D., Eicken, H., Kassens, H., Letzig, T., Reimnitz, E., Thiede, J., 1994. Sediments in Arctic sea ice: entrainment, transport and release. Mar. Geol. 119, 185–214.
Nürnberg, D., Fütterer, K., Niessen, F., Noergaard-Pedersen, N., Schubert, C.J., Spielhagen, R.F., Wahsner, M., 1995. The depositional environment of the Laptev Sea continental margin: preliminary results from the R/V Polarstern ARK IX-4 cruise. Polar Res. 14 (1), 43–53.
Nürnberg, D., Baranov, B.V., Karp, B.J., 1997. GREGORY cruise report: RV Akademik M.A. Lavrentyev Cruise 27. GEOMAR Report 60. 69 pp.
Ohtani, K., Nagata, Y., 1990. The role of the Okhotsk Sea on the formation of the Oyashio water. EOS Trans. Am. Geophys. Union 71 (28), 881.
Okazaki, Y., Takahashi, K., Yoshitani, H., Nakatsuka, T., Ikehara, M., Wakatsuchi, M., 2003. Radiolarians under the seasonally sea-ice covered conditions in the Okhotsk Sea: flux and their implications for paleoceanography. Mar. Micropal. 49, 195–230.
Okazaki, Y., Takahashi, K., Katsuki, K., Ono, A., Hori, J., Sakamoto, T., Uchida, M., Shibata, Y., Ikehara, M., Aoki, K., 2005. Late Quaternary paleoceanographic changes in the southwestern Okhotsk Sea: evidence from geochemical, radiolarian, and diatom records. Deep-Sea Res. II 52, 2332–2350.
Osterkamp, T.E., Gosink, J.P., 1984. Observations and analyses of sediment-laden sea ice. The Alaskan Beaufort Sea: Ecosystems and Environments. Academic Press Inc., pp. 73–93.
Paillard, D., Labeyrie, L., Yiou, P., 1996. Macintosh program performs time-series analysis. EOS Trans. Am. Geophys. Union 77, 379.
Parkinson, C.L., 1990. The impact of the Siberian High and Aleutian low on the sea ice cover of the Sea of Okhotsk. Ann. Glaciol. 14, 226–229.
Parkinson, C.L., Gratz, A.J., 1983. On the seasonal sea ice cover of the Sea of Okhotsk. J. Geophys. Res. 88, 2793–2802.
Parkinson, C.L., Comiso, J.C., Zwally, H.J., Cavalieri, D.J., Gloersen, P., Campbell, W.J., 1987. Arctic sea ice, 1973–1976: satellite passive-microwave observations. Scientific and Technical Information Branch, NASA SP-489, p. 296.
Pettijohn, F.J., Potter, P.E., Siever, R., 1972. Sand and Sandstone. Springer, Berlin, Heidelberg, New York. 618 pp.

Polyakov, I., Martin, S., 2000. Interaction of the Okhotsk diurnal tides with the Kashevarov Bank polynya. J. Geophys. Res. 105 (C2), 3281–3294.
Ponomorev, V., Trusenkova, O., Ustinova, E., Kaplunenko, D., 1999. Interannual variations of oceanographic and meteorological characteristics in the Sea of Okhotsk. PICES Sci. Rep. 12, 31–40.
Prell, W.L., Imbrie, J., Martinson, D.G., Morley, J.J., Pisias, N.G., Shackleton, N.J., Streeter, H.F., 1986. Graphic correlation of oxygen isotope stratigraphy application to the Late Quaternary. Paleoceanography 1, 137–162.
Rea, D.K., 1994. The paleoclimatic record provided by eolian deposition in the deep sea: the geological history of wind. Rev. Geophys. 32 (2), 159–195.
Rearic, D.M., Barnes, P., Reimnitz, E., 1990. Bulldozing and Resuspension of shallow-shelf sediment by ice keels: implications for Arctic sediment transport trajectories. Mar. Geol. 91, 133–147.
Reimnitz, E., Kempema, E., Barnes, P.W., 1987. Anchor ice, seabed freezing, and sediment dynamics in shallow Arctic Seas. J. Geophys. Res. 92 (C13), 14,671–14,678.
Reimnitz, E., Barnes, P.W., Weber, W.S., 1993a. Particulate matter in pack ice of the Beaufort Gyre. J. Glaciol. 39, 186–198.
Reimnitz, E., Clayton, J.R., Kempema, E., Payne, J.R., Weber, W.S., 1993b. Interaction of rising frazil with suspended particles: tank experiments with application to nature. Cold Reg. Sci. Technol. 21, 117–135.
Reimnitz, E., McCormick, M., McDougall, K., Brouwers, E., 1993c. Sediment export by ice rafting from a coastal polynya, Arctic Alaska, U.S.A. Arct. Alp. Res. 25 (2), 83–98.
Reimnitz, E., McCormick, M., Bischof, J., Darby, D.A., 1998. Comparing sea-ice sediment load with Beaufort sea shelf deposits: is entrainment selective? J. Sediment. Res. 68 (5), 777–787.
Riser, S.C., 1990. Sources of North Pacific Intermediate Water from the Sea of Japan and Sea of Okhotsk. EOS Trans. Am. Geophys. Union 71 (28), 881.
Sakamoto, T., Tanabe, T., Shimizu, H., Iijima, K., Ikehara, M., Kimura, N., Aoki, K., Nakatsuka, T., Wakatsuchi, M., 2003. Millennium scale sudden and abrupt sea-ice expansion events in the Sea of Okhotsk based on analysis of ice-rafted debris (IRD) in marine sediment cores. Front. Res. Earth Evol. 1, 275–278.
Sakamoto, T., Ikehara, M., Aoki, K., Iijima, K., Kimura, N., Nakatsuka, T., Wakatsuchi, M., 2005. Ice-rafted debris (IRD)-based sea-ice expansion events during the past 100 kyrs in the Okhotsk Sea. Deep-Sea Res. II 52, 2275–2301. doi:10.1016/j.dsr2.2005.08.007.
Shcherbina, A.Y., Talley, L.D., Rudnick, D.L., 2003. Direct observations of North Pacific Ventilation: brine rejection in the Okhostk Sea. Science 302, 1952–1955.
Shiga, K., Koizumi, I., 2000. Latest Quaternary oceanographic changes in the Okhotsk Sea based on diatom records. Mar. Micropaleontol. 38, 91–117.
Southon, J.R., Kashgarin, M., Gorbarenko, S., 1993. Calcite dissolution and the radiocarbon age of pre-bomb surface water in North Pacific Coastal Region, Washington. Am. Geophys. Union. 198 pp.
St. John, K.E.K., Krissek, L.A., 1999. Regional patterns of Pleistocene ice-rafted debris flux in the North Pacific. Paleoceanography 14 (5), 653–662.
Stierle, A.P., Eicken, H., 2002. Sediment inclusions in Alaskan coastal sea ice: spatial distribution, interannual variability, and entrainment requirements. Arct. Antarct. Alp. Res. 34 (4), 465–476.
Stuiver, M., Reimer, P.J., 1993. Extended ^{14}C data base and revised CALIB 3.0 ^{14}C age calibration program. In: Stuiver, M., Long, A., Kra, R.S. (Eds.), Calibration 1993: Radiocarbon, 35(1), pp. 215–230.
Svendsen, J.I., Alexanderson, H., Astakhov, V.I., Demidov, I., Dowdeswell, J.A., Funder, S., Gataullin, V., Henriksen, M., Hjort, C., Houmark-Nielsen, M., Hubberten, H.W., Ingolfson, I., Jacobsson, M., Kjær, K.H., Larsen, E., Lokrantz, H., Lunkha, J.P., Lys, A., Mangerud, J., Matiouchkov, A., Murray, A., Moeller, P., Niessen, F., Nikolskaya, O., Polyak, L., Saarnisto, M., Siegert, C., Siegert, M.J., Spielhagen, R.F., Stein, R., 2004. Late Quaternary ice sheet history of northern Eurasia. Quat. Sci. Rev. 23, 1229–1271.
Svitoch, A.A., 2003. Marine Pleistocene of the coasts of Russia (Paleogeography). Oceanology 43 (5), 742–752.
Talley, L.D., 1991. An Okhotsk Sea water anomaly: implications for ventilation in the North Pacific. Deep-Sea Res. 38 (Suppl. 1), 171–190.
Tchaibana, Y., Honda, M., Takeuchi, K., 1996. The abrupt decrease of the sea ice over the southern part of the Sea of Okhotsk in 1989 and its relation to the recent weakening of the Aleutian Low. J. Meteor. Soc. Japan 74, 579–584.
Ternois, Y., Kawamura, K., Keigwin, L., Ohkouchi, N., Nakatsura, T., 2001. A biomarker approach for assessing marine and terrigenous inputs to the sediments of Sea of Okhotsk for the last 27,000 years. Geochim. Cosmochim. Acta 65 (5), 791–802.
Tiedemann, R., Sarnthein, M., Shackleton, N.J., 1994. Astronomic timescale for the Pliocene Atlantic $\delta^{18}O$ and dust flux records of Ocean Drilling Program Site 659. Paleoceanography 9, 619–638.
van Andel, T.H., Heath, G.R., Moore, T.C., 1975. Cenozoic history and paleoceanography of the Central Equatorial Pacific Ocean. Geol. Soc. Am. Mem. 143, 49–72.
von Huene, R., Larson, E., Crouch, J., 1973. Preliminary study of ice-rafted erratics as indicators of glacial advances in the Gulf of Alaska. Initial Rep. Deep Sea Drill. Proj., 18, pp. 835–842.
Wakatsuchi, M., Martin, S., 1990. Satellite observations of the ice cover of the Kurile basin region of the Okhotsk Sea and its relation to the regional oceanography. J. Geophys. Res. 95 (C8), 13,393–13,410.
Wang, W.-C., Li, K., 1990. Precipitation fluctuation over semi-arid region in Northern China and the relationship with El Niño/Southern Oscillation. J. Climate 3, 769–783.
Wang, W.-L., Wang, L.-C., 2008. Reconstruction of oceanographic changes based on the diatom records of the central Okhotsk Sea over the last 500000 years. Terr. Atmos. Ocean. Sci. 19 (4), 403–411.
Watanabe, T., Wakatsuchi, M., 1998. Formation of 26.8–26.9 σ_θ water in the Kurile Basin of the Sea of Okhotsk as a possible origin of North Pacific Intermediate Water. J. Geophys. Res. 102 (C2), 2849–2865.
Wong, C.S., Matear, R.J., Freeland, H.J., Whitney, F.A., Bychkov, A.S., 1998. WOCE Line P1W in the Sea of Okhotsk 2. CFCs and the formation rate of intermediate water. J. Geophys. Res. 103 (C8), 15,625–15,642.
Yoneda, M., Kitagawa, H., van der Plicht, J., Uchida, M., Tanaka, A., Uehiro, T., Shibata, Y., Morita, M., Ohno, T., 2000. Pre-bomb marine reservoir ages in the western North Pacific: preliminary results on Kyoto University collection. Nucl. Instrum. Methods B172, 377–381.
Zamoruyev, V., 2004. Quaternary glaciation of north-east Asia. In: Ehlers, J., Gibbard, P.L. (Eds.), Quaternary Glaciations — Extent and Chronology. Part III. Elsevier, Netherlands, pp. 321–323.
Zech, W., Bäumler, R., Savoskul, O., Sauer, G., 1996. Zur Problematik der pleistozänen und holozänen Vergletscherung Süd-Kamtschatkas - erste Ergebnisse bodengeographischer Untersuchungen, Eiszeitalter und Gegenwart, 46, pp. 132–143.
Zech, W., Bäumler, R., Savoskul, O., Braitseva, O.A., Meleketsev, J., 1997. Evidence of middle Pleistocene glaciation in SW-Kamchatka. Zeitschr. Gletscherkde. Glazialgeol. 33 (1), 15–20.
Zenkevitch, L.A., 1963. Biology of the Seas of the USSR. Wiley-Interscience, New York, N.Y. 995 pp., (translated from Russian).